

1 Eruptive history and $^{40}\text{Ar}/^{39}\text{Ar}$ geochronology of the Milos volcanic 2 field, Greece

3
4 Xiaolong Zhou¹, Klaudia Kuiper¹, Jan Wijbrans¹, Katharina Boehm¹, Pieter Vroon¹

5 ¹Department of Earth Sciences, VU University Amsterdam, De Boelelaan 1085, 1081 HV Amsterdam, The Netherlands.

6 *Correspondence to:* Xiaolong Zhou (z.x.l.zhou@vu.nl)

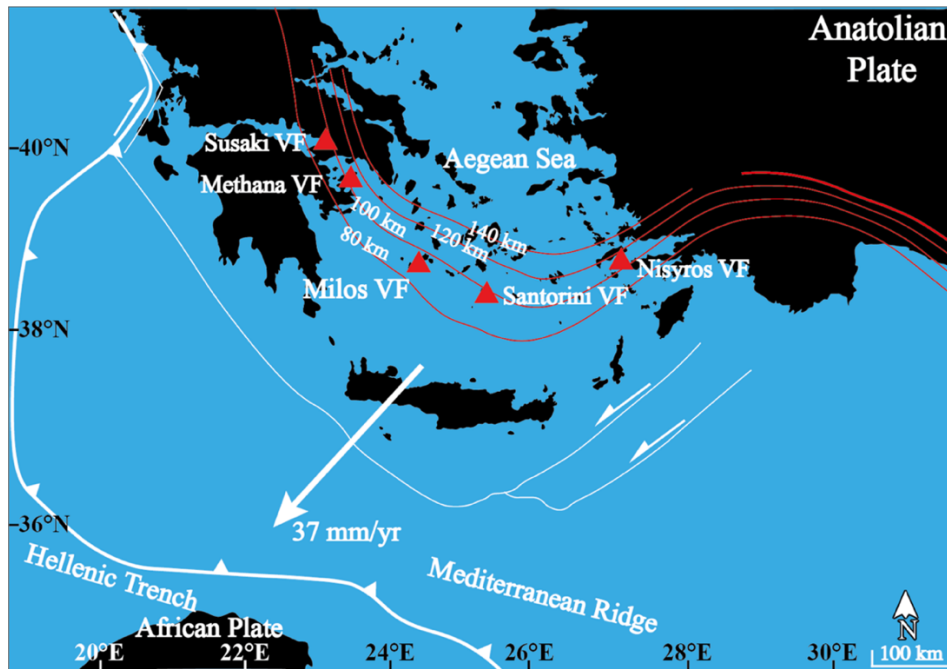
7 **Abstract.** High-resolution geochronology is essential for determining the growth-rate of volcanoes, which is one of the key
8 factors for establishing the periodicity of volcanic eruptions. However, there are less high-resolution eruptive histories ($>10^6$
9 years) determined for long-lived submarine arc volcanic complexes than for subaerial complexes, since submarine volcanoes
10 are far more difficult to observe than subaerial ones. In this study, high-resolution geochronology and major element data are
11 presented for Milos Volcanic Field (VF) in the South Aegean Volcanic Arc, Greece. The Milos VF has been active for over 3
12 Ma, and the first two million years of its eruptive history occurred in a submarine setting that has been emerged above sea
13 level. The long submarine volcanic history of the Milos VF makes it an excellent natural laboratory to study the growth-rate
14 of a long-lived submarine arc volcanic complex. This study reports twenty-one new high-precision $^{40}\text{Ar}/^{39}\text{Ar}$ ages and major
15 element compositions for eleven volcanic units of the Milos VF. This allows us to divide the Milos volcanic history into at
16 least three periods of different long-term volumetric volcanic output rate (Q_e). Period I (submarine, ~ 3.3 -2.13 Ma) and III
17 (subaerial, 1.48 Ma-present) have low Q_e of $0.9 \pm 0.5 \times 10^{-5} \text{ km}^3 \cdot \text{yr}^{-1}$ and $0.25 \pm 0.05 \times 10^{-5} \text{ km}^3 \cdot \text{yr}^{-1}$, respectively. Period II
18 (submarine, 2.13 - 1.48 Ma) has a 3-12 times higher Q_e of $3.0 \pm 1.7 \times 10^{-5} \text{ km}^3 \cdot \text{yr}^{-1}$. The Q_e of the Milos VF is 2-3 orders of
19 magnitude lower than the average for rhyolitic systems and continental arcs.

20 1 Introduction

21 Short-term eruptive histories and compositional variations of lavas and pyroclastic deposits of many arc volcanic fields are
22 well established. However, high-resolution eruptive histories that extend back $> 10^5$ - 10^6 years have been determined only for
23 a handful of long-lived subaerial arc volcanic complexes. Some examples are: Mount Adams (Hildreth and Lanphere, 1994),
24 Tatará–San Pedro (Singer et al., 1997), Santorini (Druitt et al., 1999), Montserrat (Cole et al., 2002), Mount Baker (Hildreth
25 et al., 2003a), Katmai (Hildreth et al., 2003b), and Ceboruco–San Pedro (Frey et al., 2004). To establish the growth-rate of
26 volcanic complexes and disentangle the processes responsible for the eruption, fractionation, storage, and transport of magmas
27 over time, comprehensive geological studies are required. These include detailed field mapping, sampling, high-resolution
28 geochronology and geochemical analysis. Based on these integrated studies, the growth-rate of volcanoes can be determined
29 to establish the periodicity of effusive and explosive volcanism.

30 The Milos Volcanic Field (VF) is a long-lived volcanic complex that has been active for over 3 Ma. The Milos VF erupted for
31 a significant part of its life below sea level, similar to the other well studied volcanic structures in the eastern Mediterranean
32 (Fytikas et al., 1986; Stewart and McPhie, 2006). The eruptive history of the Milos VF has been examined with a broad range
33 of chronostratigraphic techniques such as K-Ar, U-Pb, fission track, ^{14}C and biostratigraphy (e.g. Angelier et al., 1977, Fytikas
34 et al., 1976, 1986, Traineau and Dalabakis, 1989, Matsuda et al., 1999, Stewart and McPhie, 2006, Van Hinsbergen et al., 2004
35 and Calvo et al., 2012). However, most of the published ages have been measured using the less precise K-Ar or fission track
36 methods, and modern, high precision $^{40}\text{Ar}/^{39}\text{Ar}$ ages for the Milos VF have not been published so far. In this study, (1) we
37 provide high-precision $^{40}\text{Ar}/^{39}\text{Ar}$ geochronology of key volcanic units of the Milos VF and (2) refine the stratigraphic

38 framework of the Milos VF with the new high-precision $^{40}\text{Ar}/^{39}\text{Ar}$ ages and major element composition. (3) We also quantify
39 and constrain the compositional and volumetric temporal evolution of volcanic products of the Milos VF.



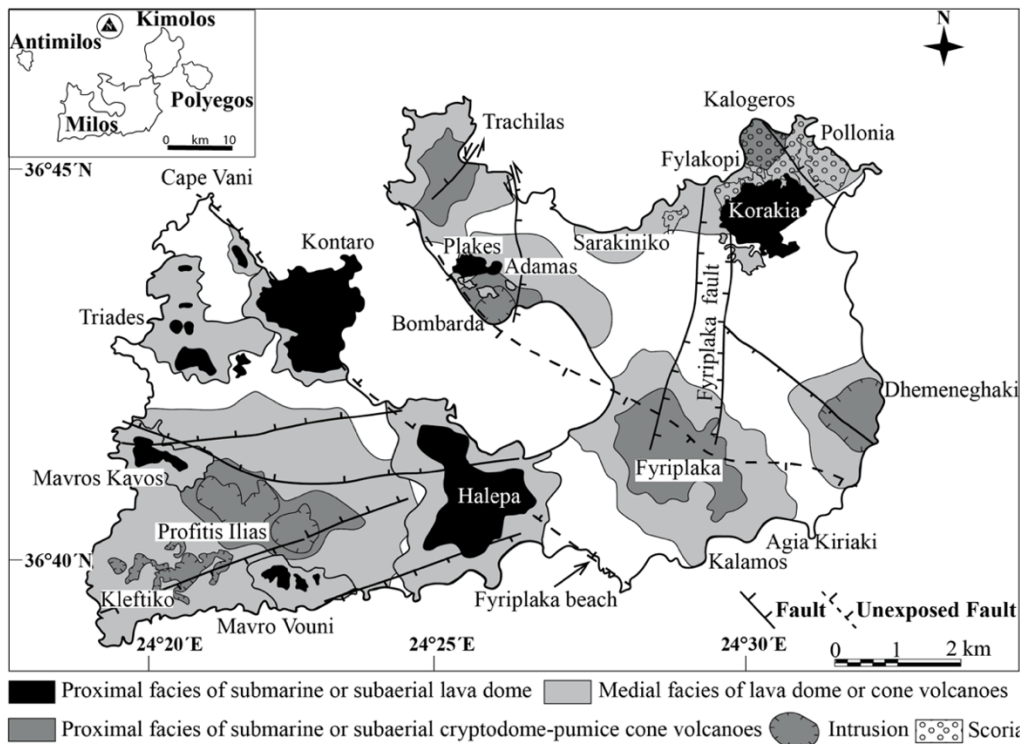
40
41 **Figure 1. Map of the South Aegean Volcanic Arc (SAVA). Red triangles indicate Volcanic Fields (VF): Susaki, Methana and Milos**
42 **VFs in the western SAVA, Santorini VF in the centre and Nisyros VF in the eastern SAVA. Red contour lines show the depth to**
43 **the Benioff zone (Hayes et al., 2018). The white arrow represents the GPS-determined plate velocity of the Aegean microplate**
44 **relative to the African plate from Doglioni et al. (2002).**

45 1.1 Geological setting

46 The Milos VF is part of the South Aegean Volcanic Arc (SAVA), an arc which was formed in the eastern Mediterranean by
47 subduction of the African plate beneath the Aegean microplate (Figure 1, Nicholls, 1971; Spakman et al., 1988; Duermeijer et
48 al., 2000; Pe-Piper and Piper, 2007; Rontogianni et al., 2011). The present-day Benioff zone is located approximately 90 km
49 underneath Milos (Hayes et al., 2018). The upper plate is influenced by extensional tectonics (e.g. McKenzie, 1978; Pe-Piper
50 and Piper, 2013), which is evident on the island of Milos as horst and graben structures (Figure 2).

51 The Milos VF is exposed on the islands of the Milos archipelago: Milos, Antimilos, Kimolos and Polyegos. The focus of this
52 study is Milos which has a surface area of 151 km². The geology and volcanology of Milos have been extensively studied in
53 the last 100 years. The first geological map was produced by Sonder (1924). This work was extended by Fytikas et al. (1976)
54 and Angelier et al. (1977) and the subsequent publications of Fytikas et al. (1986) and Fytikas (1989). Interpretations based on
55 volcanic facies of the complete stratigraphy were made by Stewart and McPhie (2003, 2006). More detailed studies of single
56 volcanic centres (e.g. Bombarda volcano and Fyriplaka complex) were published by Campos Venuti and Rossi (1996) and
57 Rinaldi et al. (2003). Milos has also been extensively studied for its epithermal gold mineralization, summarized by Alfieris
58 et al. (2013). Milos was known during the Neolithic period for its export of high-quality obsidian. Today the main export
59 product is kaolinite mined from hydrothermally altered felsic volcanic units in the centre of the island (e.g. Alfieris et al.,
60 2013).

61 The geology of Milos can be divided into four main units: (1) metamorphic basement, (2) Neogene sedimentary rocks, (3)
62 volcanic sequences and (4) the alluvial cover. The metamorphic basement crops out at the southwest, south and southeast of
63 Milos (Figure 3) and is also found as clasts in many volcanic units. The metamorphic rocks include lawsonite-free jadeite
64 eclogite, lawsonite eclogite, glaucophane schist, quartz-muscovite-chlorite and chlorite-amphibole schist (Fytikas et al., 1976,
65 1986; Grasemann et al., 2018; Kornprobst et al., 1979). The exposed units belong to the Cycladic Blueschist Unit (Lower
66 Cycladic nappe), whereas eclogite pebbles in the phreatic eruption products called “green lahar” by Fytikas (1977) are derived
67 from the Upper Cycladic Nappe (Grasemann et al., 2018).



68

69

70

71

Figure 2. Distribution of the proximal and medial facies of the submarine pumice cone/cryptodome volcanoes, submarine, submarine-subaerial and subaerial domes and rhyolitic complexes (tuff cone and associated lava) of Milos, modified after Fytikas et al. (1986) and Stewart and McPhie (2006). The distal facies of Stewart and McPhie (2006) is not shown.

72

73

74

75

76

77

78

79

80

81

82

On top of this metamorphic basement, Neogene fossiliferous marine sedimentary rocks were deposited (e.g. Van Hinsbergen et al. 2004). This sedimentary sequence can be divided into a lower unit A and upper unit B that is unconformably overlain by volcanoclastic sediments (Van Hinsbergen et al., 2004). Unit A is 80 m thick and consists of fluvatile-lacustrine, brackish and shallow marine conglomerate, sandstone, dolomite and limestone. Unit B is 25-60 m thick and consists of sandstone overlain by a succession of alternating marls and sapropels, suggesting a deeper marine setting (Van Hinsbergen et al., 2004). Five volcanic ash layers that contain biotite are found in this Neogene sedimentary sequence, either suggesting that volcanic eruptions in small volume already occurred in the Milos area or that these ash layers are derived from larger eruptions of volcanic centres further away from Milos (van Hinsbergen et al., 2004). Age determinations by bio-magneto- and cyclostratigraphy suggested that deposition of Unit A started at approximately 5 Ma, and that Milos subsided 900 m in 0.6 Ma (Van Hinsbergen et al. 2004) due to extension. This subsidence happened ca 1.0-1.5 Ma before the onset of the main phase of Pliocene- recent volcanism on Milos.

83

84

85

86

87

88

89

90

91

The Pliocene-recent volcanic sequence of Milos has been subdivided into different units by Angelier et al. (1977) and Fytikas et al. (1986). In addition, Stewart and McPhie (2006) provided a detailed facies analysis of the different volcanic units. The subdivision by Angelier et al. (1977) is not constrained well due to their limited amount of age data. The subdivision of volcanic units by Fytikas et al. (1986) and facies descriptions of Stewart and McPhie (2006) are summarized below. It is important to note that according to Stewart and McPhie (2006), the five volcanic cycles described by Fytikas et al. (1986) are difficult to match with existing age data and the continuous progression in volcanic construction (Fig. 4). For example, the first phase of Fytikas et al. (1986), the Basal Pyroclastic Series, contains the large pumice cone-cryptodome volcanoes according to Stewart and McPhie (2006). Two of these pumice-cone cryptodome volcanoes are much younger and intercalated between the Complex of Domes and Lava Flows (CDLF) of Fytikas et al. (1986).

92

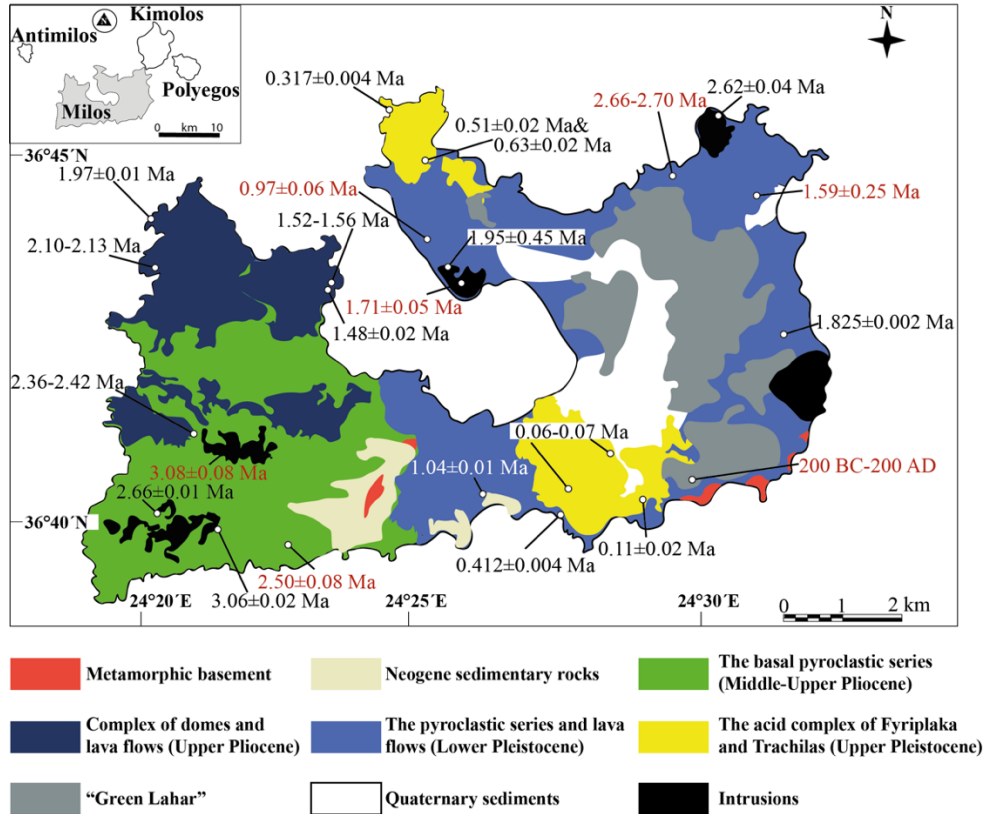
93

94

95

The first volcanic unit deposited in the Milos area is the Basal Pyroclastic Series (BPS) (Fytikas et al., 1986) or submarine felsic cryptodome-pumice cone volcanoes (Stewart and McPhie, 2006, Figure 2-4). This unit consists of thickly bedded pumice breccia with a rhyolitic-dacitic composition. These rhyolites-dacites are aphyric or contain quartz-feldspar±biotite phenocrysts. Graded sandstone and bioturbated and fossil rich (in-situ bivalve shells) mudstone are intercalated, indicating a marine

96 environment and a water depth of several hundreds of meters (e.g. Stewart, 2003; Stewart and McPhie, 2006), whereas later
 97 degassed magmas with a similar composition intruded as sills and cryptodomes. The BPS has been strongly affected by
 98 hydrothermal fluids, especially the proximal deposits (e.g. Kiliias et al., 2001).



99
 100 **Figure 3. Simplified geological map of Milos with our ⁴⁰Ar/³⁹Ar ages and sample locations of key volcanic deposits, modified after**
 101 **Stewart and McPhie (2006) and Grasmann et al. (2018). The stratigraphic units of Milos are from Fytikas et al. (1986). Age data**
 102 **from this study are in black, published ages are shown in red (Angelier et al., 1977, Fytikas et al., 1986, Traineau and Dalabakis,**
 103 **1989, and Stewart and McPhie, 2006). The “Green Lahar” (Fytikas, 1977) consists of deposits from multiple phreatic explosions**
 104 **and contains fragments of metamorphic, sedimentary and volcanic rocks.**

105 The second volcanic unit was named the Complex of Domes and Lava Flows (CDLF, Fytikas et al., 1986) and the volcanic
 106 facies of this unit are described as the submarine dacitic and andesitic domes by Stewart and McPhie (2006). This phase of
 107 effusive submarine volcanism was predominantly andesitic/dacitic in composition and produced microcrystalline rocks with
 108 phenocrysts of pyroxene, amphibole, biotite and plagioclase. The eruption centres were mainly located along NNE faults and
 109 formed up to 300 m thick deposits extending over areas of 2.5 to 10 km² around the eruption centres. In the north-eastern part
 110 of Milos, an andesitic scoria cone provided scoria lapilli and bombs to deeper water settings. Sandstone intercalated in the
 111 CDLF contains both igneous and metamorphic minerals suggesting input from the basement. Rounded pebbles of rhyolite and
 112 dacite indicate that some of the volcanic deposits were above sea level, or in very shallow, near shore environments (e.g.
 113 Stewart and McPhie, 2006).

114 The third volcanic unit is called the Pyroclastic Series and Lava Domes (PSLD) by Fytikas et al. (1986) and belongs to
 115 submarine-to-subaerial dacitic and andesitic lava domes of Stewart and McPhie (2006). This highly variable group is
 116 dominated by rhyolitic, dacitic and andesitic lavas, domes, pyroclastic deposits and felsic pumiceous sediments (Stewart and
 117 McPhie, 2006). Thickness varies between 50-200 m, and the deposits are located in the eastern and northern parts of Milos
 118 (Figure 2 and 3). The initial pyroclastic layers were subaqueously deposited and the extrusion of a dome resulted in the
 119 deposition of talus around the margins by mass flow. On top of the dome sand- and siltstone with fossils (Ostrea fossil
 120 assemblage) and traction-current structures suggest that the top of the dome was above wave base. The youngest deposits of
 121 this unit are dacitic and andesitic lavas and domes. These domes generated subaerial block-and-ash flow and surge deposits.
 122 Paleosols within these deposits are a clear indicator that some areas were above sea level. The last unit of the PSLD is

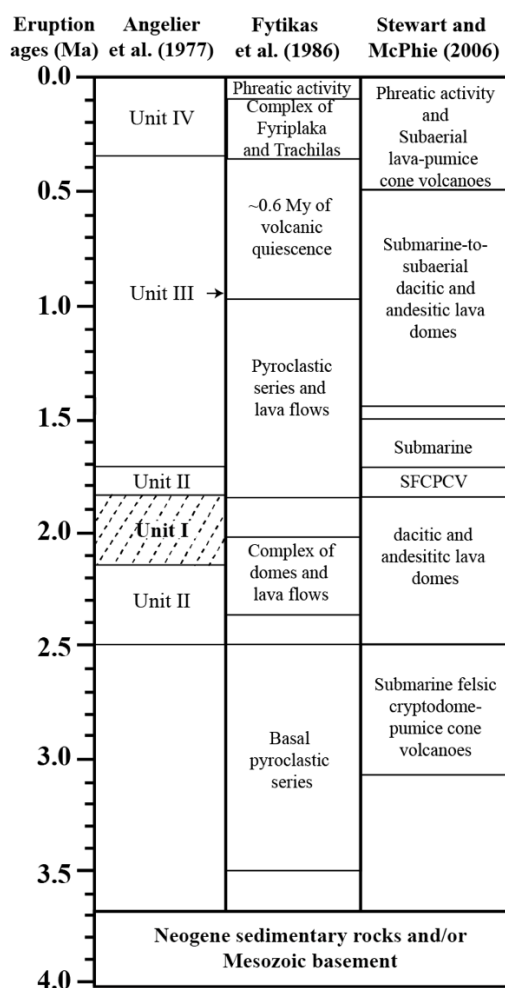
123 represented by large subaerial rhyolitic lava that contains quartz and biotite phenocrysts and is found near Halepa in the south-
 124 central part of Milos.

125 **Table 1. Published eruption ages of stratigraphic units of the island of Milos**

Stratigraphy	Sample	Mineral	Location	Petrology	K ₂ O (wt.%)	Age (Ma)	± 1σ	Reference
Unit IV	Angelier_1	Unknown	Fyriplaka	Rhyolite	-	-	-	
Unit III	Angelier_2	Unknown	Halepa	Rhyolite	2.44	0.95	0.06	
Unit II	Angelier_3	Unknown	Triades	Dacite	1.47	1.71	0.08	Angelier et al. (1977)
	Angelier_4	Unknown	Kleftico	Andesite	1.77	2.33	0.09	
	Angelier_5	Unknown	Kleftico	Andesite	1.45	2.50	0.09	
Unit I	Angelier_6	Unknown	Adamas	Rhyolite	2.90	2.15	0.08	
	Angelier_7	Unknown	Dhemenehaki	Rhyolite	2.75	1.84	0.08	
Phreatic activity	Gif-7358&7359	Carbonized wood	Agia Kiriaki	Lahar deposits	-	200 BC-200 AD		Trainau and Dalabakis (1989)
CFT	M196	Unknown	Fyriplaka	Rhyolite	2.9	0.09	0.02	Fytikas et al. (1976, 1986)
	M194	Unknown	Fyriplaka	Rhyolite	2.85	0.14	0.03	
	M168	Unknown	Trachilas	Rhyolite	3.91	0.37	0.09	
	M-48	Biotite	NW of Filiplaka	Rhyolite	6.41	0.48	0.05	
PSLD	M-OB1	Groundmass	N of Dhemenehaki	Obsidian	2.53	0.88	0.18	Fytikas et al. (1976, 1986)
	M27	Unknown	Plakes	Dacite	1.87	0.97	0.06	
	M-OB2	Groundmass	Bombarda	Obsidian	2.73	1.47	0.05	
	M103	Unknown	near Pollonia	Andesite	1.87	1.59	0.25	
	M146	Unknown	1km NW of Adamas	Rhyolite	3.09	1.71	0.05	
	M110	Unknown	Sarakiniko	Dacite	2.57	1.85	0.10	Matsuda et al. (1999)
	MI-1	Lava	Plakes	Dacite	2.07	0.80	0.10	
	MI-4	Lava	Plakes	Dacite	2.32	1.20	0.10	
	MIL130	Zircon	Triades	Dacite	-	1.44	0.08	Stewart and McPhie (2006)
	Fission track1	Groundmass	Adamas	Obsidian	-	1.54	0.18	Bigazzi and Radi (1981)
Fission track2	Groundmass	Bombarda	Obsidian	-	1.57	0.15		
Fission track3	Groundmass	Bombarda-Adamas	Obsidian	-	1.57	0.12	Arias et al. (2006)	
Fission track3	Groundmass	Dhemenehaki	Obsidian	-	1.60	0.06		
CDLF	M1	Unknown	Aghios, near Triades	Rhyolite	3.32	2.04	0.09	Fytikas et al. (1976, 1986)
	M66	Unknown	~1 km NW of Adamas	Dacite	2.61	2.03	0.06	
	M156	Unknown	Angathia, near Triades	Dacite	2.84	2.38	0.10	
MIL243	Zircon	Triades	Dacite	-	2.18	0.09	Stewart and McPhie (2006)	
BPS	MIL365	Zircon	Filakopi	Rhyolite	-	2.66	0.07	Stewart and McPhie (2006)
	MIL343	Zircon	Kalogeros cryptodome	Dacite	-	2.70	0.04	
	M164	Unknown	Kleftico	Rhyolite	2.84	3.08	0.08	Fytikas et al. (1976, 1986)
	M163	Unknown	Kleftico	Andesite	1.18	3.50	0.14	

126 Angelier et al. (1977) do not provide sample names, only numbers for the sample locations. Here the location is given after “Angelier_”
 127 (Angelier et al. 1977, their Fig. 3). Abbreviations: BPS=Basal pyroclastic series; CDLF=Complex of domes and lava flows;
 128 PSLD=Pyroclastic series and lava domes; CTF=Complexes of Trachilas and Fyriplaka. See more details in Figure. 4.

129 The fourth unit consists of the subaerially constructed rhyolitic Complexes of Trachilas and Fyriplaka (CTF) (Fytikas et al.,
 130 1986), which Stewart and McPhie (2006) interpreted as subaerial rhyolitic lava-pumice cones. These two volcanic complexes
 131 are built from rhyolitic pumice deposits and lavas that contain quartz and biotite phenocrysts (10-20 modal %). The deposits
 132 have a maximum thickness of 120 m and decrease to several meters thickness in the distal parts. Basement-derived schist is
 133 found as lithic clasts (Fytikas et al., 1986). In addition, the Kalamos rhyolitic lava dome, which outcrops on the southern coast
 134 of Milos, produced lava that spread westwards to the Fyriplaka beach (Figure 2). This lava belongs to this fourth phase and is
 135 probably derived from an older volcano and not the Fyriplaka complex (Campos Venuti and Rossi, 1996).
 136 The fifth volcanic unit comprises deposits from phreatic activity, especially in the northern part of the Zefiria Graben and near
 137 Agia Kiriaki (Figure 2 of Stewart and McPhie, 2006). Many overlapping craters are surrounded by lithic breccias that are
 138 composed of variably altered metamorphic basement clasts and volcanic clasts. This phreatic activity has continued into
 139 historic times (Trainau and Dalabakis, 1989). Fytikas et al. (1986) referred to this unit as “green lahar”, although it indicated
 140 that this deposit is not a lahar but the product of phreatic eruptions in the last 0.2 Ma.



141
 142 **Figure 4. Previous proposed stratigraphic frameworks for Milos by Angelier et al. (1977), Fytikas et al. (1986) and Stewart and**
 143 **McPhie (2006). Volcanic unit II of Angelier et al. (1977) contains unit I. Stewart and McPhie (2006) described the volcanic faces of**
 144 **Milos mainly based on the geochronological works of Angelier et al. (1977) and Fytikas et al. (1986). Abbreviation:**
 145 **SFCPCV=Submarine felsic cryptodome-pumice cone volcanoes.**

146 **1.2 Previous geochronological studies**

147 Previous geochronological work is summarised in Table 1. Angelier et al. (1977) reported six K-Ar ages (0.95-2.50 Ma). These
 148 ages were used in combination with field observations to divide the Milos volcanic succession into four units. However, the
 149 samples from Fyriplaka, the fourth unit, were too young to be dated by Angelier et al. (1977). Fytikas et al. (1976, 1986)
 150 published 16 K-Ar ages for Milos (0.09-3.50 Ma) including an age of 0.09-0.14 Ma for the Fyriplaka complex. Fytikas et al.
 151 (1986) also obtained 3 K-Ar ages for Antimilos (0.32 ± 0.05 Ma), Kimolos (3.34 ± 0.06 Ma) and Polyegos (2.34 ± 0.17 Ma).

152 Trainau and Dalabakis (1989) dated the very young phreatic deposits by ^{14}C dating and found ages between 200 BC and 200
153 AD. Matsuda et al. (1999) published two K-Ar ages of 0.8 ± 0.1 (MI-1) and 1.2 ± 0.1 Ma (MI-4) for the Plakes dome that was
154 also studied by Fytikas et al. (1986). Bigazzi and Radi (1981) published two fission track ages of 1.54 ± 0.18 and 1.57 ± 0.15
155 Ma for obsidians of Bombarda-Adamas and Demenaghaki, respectively. Later fission track studies by Arias et al. (2006) (1.57
156 ± 0.12 and 1.60 ± 0.06 Ma) confirmed these ages. The fission track ages are younger than the K-Ar ages given by Angelier et
157 al. (1977; 1.84 ± 0.08 Ma for Demenaghaki) and Fytikas et al. (1986; 1.71 ± 0.05 Ma for Bombarda). In the most recent
158 geochronological study of the Milos VF, Stewart and McPhie (2006) published 4 SHRIMP U/Pb zircon ages: Triades dacite
159 facies (1.44 ± 0.08 and 2.18 ± 0.09 Ma), Kalogeros cryptodome (2.70 ± 0.04 Ma) and the Fylakopi Pumice Breccia ($2.66 \pm$
160 0.07 Ma). All uncertainties reported here are one standard deviation uncertainties as reported in the original publications,
161 except for the ^{14}C ages for which uncertainties were not specified.

162 The previous geochronological work for the MVF is mainly based on K-Ar ages. However, K-Ar ages may show undesirable
163 and unresolvable scatter due to various problems: (1) inaccurate determination of radiogenic argon due to either incorporation
164 of excess argon or incomplete degassing of argon during the experiments; (2) inclusion of cumulate or wall rock phenocrysts
165 in bulk analyses; (3) disturbance of a variety of geological processes such as slow cooling, thermal reheating; (4) unrecognized
166 heterogeneities due to separate measurements of potassium and argon content by different methods; (5) requirement of
167 relatively large quantities (milligrams) of pure sample (e.g. Lee, 2015). In addition to these methodological issues, in the case
168 of Milos we observe that hydrothermal alteration caused substantial kaolinitisation, in particular the felsic volcanic samples,
169 that most likely has affected the K-Ar systematics. Some of these issues are also valid for the $^{40}\text{Ar}/^{39}\text{Ar}$ method. However, the
170 K-Ar method does not allow testing if ages are compromised.

171 $^{40}\text{Ar}/^{39}\text{Ar}$ ages only need isotopes of argon to be measured from a single aliquot of sample with the same equipment that can
172 eliminate some of the problems with sample inhomogeneity. Furthermore, step heating and multiple single fusion experiments
173 can shed light on sample inhomogeneity due to partial alteration effects. The high sensitivity of modern noble gas mass
174 spectrometers for $^{40}\text{Ar}/^{39}\text{Ar}$ measurements results in very small sample amounts needed for analysis, that can yield more
175 information on the thermal or alteration histories than larger samples. Moreover, other argon isotopes (^{36}Ar , ^{37}Ar and ^{38}Ar) can
176 be used to infer some information about the chemical compositions (i.e. Ca and Cl) of samples. A high-resolution laser
177 incremental heating method of $^{40}\text{Ar}/^{39}\text{Ar}$ dating allows us to resolve the admixture of phenocryst-hosted inherited ^{40}Ar in the
178 final temperature steps of the incremental step heating experiments.

179 **2 Methods**

180 **2.1 Mineral separation and sample preparation**

181 Samples were collected from all major volcanic units on Milos island based on the studies of Fytikas et al. (1986), Stewart and
182 McPhie (2006) and our own observations in the field. Photos of the sample locations and thin sections can be found in
183 supplementary material I. Approximately 2 kg of fresh pumice clasts or lava was sampled from each unit. Samples were cut
184 into $\sim 5\text{ cm}^3$ cubes using a diamond saw to remove potentially altered surfaces and obtain the fresh interior parts. These cubes
185 were ultra-sonicated for 30 minutes in demi-water to remove dust and seawater and dried in an oven overnight at $50\text{ }^\circ\text{C}$. Dry
186 sample cubes were crushed in a steel jaw crusher, and this fraction was split into two portions of roughly equal size. One of
187 them was powdered in an agate shatter box and agate ball mill to a grain size of less than $2\text{ }\mu\text{m}$ for the major-element analysis.
188 The second fraction was sieved to obtain a grain size of $250\text{-}500\text{ }\mu\text{m}$ for $^{40}\text{Ar}/^{39}\text{Ar}$ dating.

189 Heavy liquids density separation techniques (IJlst, 1973) were used to purify mineral separates (groundmass, biotite, amphibole)
190 required for the $^{40}\text{Ar}/^{39}\text{Ar}$ dating. Different densities of heavy liquids were used to obtain groundmass ($2700 \leq \rho \leq 3000\text{ kg.m}^{-3}$),
191 biotite ($2900 \leq \rho \leq 3100\text{ kg.m}^{-3}$) and/or amphibole ($\sim 3100 \leq \rho \leq 3200\text{ kg.m}^{-3}$). A Franz Isodynamic Magnetic separator was
192 used to remove the magnetic minerals from the non-magnetic minerals and groundmass. The samples for $^{40}\text{Ar}/^{39}\text{Ar}$ analysis

193 were purified by handpicking under a binocular optical microscope to select mineral grains without visible alteration and
194 inclusions.

195 2.2 $^{40}\text{Ar}/^{39}\text{Ar}$ dating

196 The mineral and groundmass samples were wrapped in either 6- or 9-mm aluminium foil and packed in 20 mm aluminium
197 cups, that were vertically stacked. Based on stratigraphy and previous geochronological constraints >1 Ma samples and the <1
198 Ma samples were irradiated for 7 and 1 hours respectively in irradiation batches VU108 and VU110 in the Cadmium-Lined
199 in-Core Irradiation Tube (CLICIT) facility of the Oregon State University Training Research, Isotopes, General Atomics
200 (TRIGA) reactor. The neutron flux for all irradiations was monitored by standard bracketing using the Drachenfels sanidine
201 (DRA; 25.52 ± 0.08 Ma, modified from Wijbrans et al., 1995 and calibrated relative to Kuiper et al., 2008) and Fish Canyon
202 Tuff sanidine (FCs; 28.201 ± 0.023 Ma, Kuiper et al., 2008) with Min et al. (2000) decay constants.

203 In total, 24 samples (8 groundmasses, 15 biotites and 2 amphiboles, for sample G15M0026 both biotite and amphibole were
204 analysed) were measured by either $^{40}\text{Ar}/^{39}\text{Ar}$ fusion and/or incremental heating techniques. For incremental heating
205 experiments, 80-100 grains per sample were loaded into a 25-hole (surface per hole ~ 36 mm²) copper tray together with single
206 grain standards in ~ 12 mm² holes. The tray was prebaked in vacuum (10^{-5} - 10^{-6} mbar) at 250 °C overnight to remove
207 atmospheric argon and subsequently baked overnight at 120 °C in the ultra-high vacuum sample chamber ($<5 \times 10^{-9}$ mbar) and
208 purification system connected to a Thermo Scientific Helix MC mass spectrometer.

209 Samples and standards were heated with a focused laser beam at 8 % power using a 50W CW CO₂ laser. The released gas was
210 cleaned by exposure to a cold trap cooled by a Lauda cooler at -70 °C, a SAES NP10 at 400 °C, Ti sponge at 500 °C and cold
211 SAES ST172 Fe-V-Zr sintered metal. The five isotopes of argon were measured simultaneously on five different collectors:
212 ^{40}Ar on the H2-Faraday, ^{39}Ar on the H1-Faraday or the H1-CDD, ^{38}Ar on the AX-CDD, ^{37}Ar on the L1-CDD and ^{36}Ar on the
213 L2-CDD for 15 cycles with 33 seconds integration time (CDD: compact discrete dynodes). The Faraday cups on H2 and H1
214 were equipped with 10^{13} Ω amplifiers. Procedural blanks were measured every 2 or 3 analyses in different sequences, and air-
215 shots were measured every 8-12 hours to correct the instrumental mass discrimination. Gain between different collectors was
216 monitored by measuring CO₂ on mass 44 in dynamic mode on all collectors. Gain was generally stable over periods of weeks.
217 Note that because samples, standards and air calibration runs are measured during the same period, gain correction does not
218 substantially change the final age results. The raw mass spectrometer data output was converted by an in-house designed Excel
219 macro script to be compatible with the ArArCalc 2.5 data reduction software (Koppers, 2002). The $^{40}\text{Ar}/^{36}\text{Ar}$ atmospheric air
220 value of 298.56 from Lee et al. (2006) is used in the calculations. The correction factors for neutron interference reactions are
221 $(2.64 \pm 0.02) \times 10^{-4}$ for $(^{36}\text{Ar}/^{37}\text{Ar})_{\text{Ca}}$, $(6.73 \pm 0.04) \times 10^{-4}$ for $(^{39}\text{Ar}/^{37}\text{Ar})_{\text{Ca}}$, $(1.21 \pm 0.003) \times 10^{-2}$ for $(^{38}\text{Ar}/^{39}\text{Ar})_{\text{K}}$ and (8.6 ± 0.7)
222 $\times 10^{-4}$ for $(^{40}\text{Ar}/^{39}\text{Ar})_{\text{K}}$. All uncertainties are quoted at the 1σ level and include all analytical errors (i.e. blank, mass
223 discrimination and neutron interference correction and analytical error in J-factor, the parameter associated with the irradiation
224 process).

225 A reliable plateau age is defined as experiments with at least 3 consecutive steps overlapping at 2-sigma, containing >50% of
226 the $^{39}\text{Ar}_{\text{K}}$, a Mean Square Weighted Deviate (MSWD) value <2.5, and with a $^{40}\text{Ar}/^{36}\text{Ar}$ inverse isochron intercept that does not
227 deviate from atmospheric argon at 2-sigma. All the inverse isochron ages used the same steps as used in the weighted mean
228 ages, and all relevant analytical data for the age calculations following standard practices (Schaen et al., 2020) can be found
229 in supplementary material II.

230 2.3 Whole-rock major element analysis by XRF

231 Major-element concentrations were measured by X-ray fluorescence spectroscopy (XRF) on a Panalytical AxiosMax. A
232 Panalytical Eagon2 was used to create 40mm fused glass beads of Li₂B₄O₇/LiBO₂ (65.5:33.5%, Johnson & Johnson
233 Spectroflux 110) with a 1:6 dilution sample-flux ratio that were molten at 1150 °C. Sample powders were ignited at 1000 °C

234 for 2 hours to determine loss on ignition (LOI) before being mixed with the $\text{Li}_2\text{B}_4\text{O}_7/\text{LiBO}_2$ flux. Interference corrected spectra
235 intensities were converted to oxide-concentrations against a calibration curve consisting of 30 international standards. The
236 precision, expressed as the coefficient of variation (CV), is better than 0.5%. The accuracy, as measured on the international
237 standards AGV-2, BHVO-2, BCR-2 and GSP-2 was better than 0.7% (1 RSD) (supplementary material III).

238 2.4 Eruption volume calculation

239 The minimum and/or maximum eruption volume of each volcano during each eruption period is derived from the ranges of
240 thickness and surface areas that are reported in Campos and Rossi (1996) and Stewart and McPhie (2006). We converted these
241 volumes to Dense Rock Equivalent (DRE) based on the magma type of different deposits. This analysis only includes the
242 onshore deposits and results in a smaller estimate for larger pyroclastic volumes. The DRE volume is calculated using the
243 equation of Crosweller et al. (2012):

$$244 \quad DRE (km^3) = \frac{tephra \text{ vol } (km^3) \times tephra \text{ density } (kg/m^3)}{magma \text{ density } (kg/m^3)}$$

245 Tephra density is assumed to be 1000 kg/m^3 (Crosweller et al., 2012). Magma density varies depending on the magma type.
246 Here we used 2300 kg/m^3 for rocks with a SiO_2 range of 65-77 wt.% and 2500 kg/m^3 for all samples with $\text{SiO}_2 < 65 \text{ wt.}\%$.
247 DRE corresponds to the unvesiculated erupted magma volume. Therefore, we did not convert the volume of some cryptodome
248 and lavas from Profitis Illias (G15M0017), Triades (G15M0021-24), Dhemenehaki (G15M0032B) and Halepa (G15M0013)
249 to the DRE since they contain less than 5% vesicles.

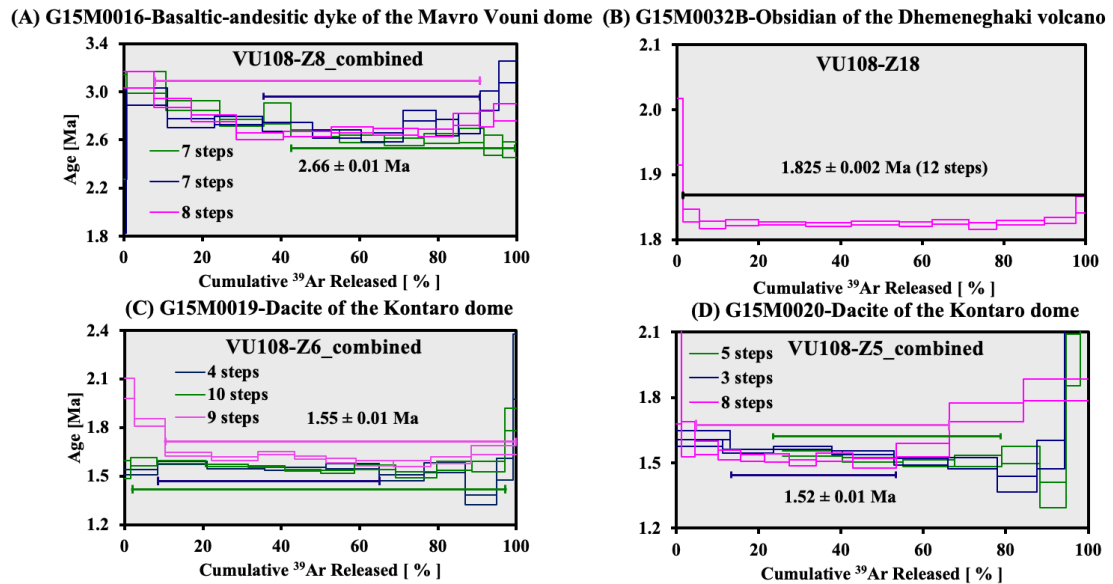
250 3 Results

251 3.1 $^{40}\text{Ar}/^{39}\text{Ar}$ age results

252 In this section, we present our groundmass, biotite and amphibole $^{40}\text{Ar}/^{39}\text{Ar}$ results for eleven volcanic units of Milos. The
253 $^{40}\text{Ar}/^{39}\text{Ar}$ ages range from 0.06 to 4.10 Ma and cover most of the major volcanic units of Milos. Table 2 and 3 show the
254 $^{40}\text{Ar}/^{39}\text{Ar}$ results of incremental heating steps and single grain fusion analyses, respectively. Note that the Irr-ID column in
255 these two Tables represents the irradiation ID of the analytical experiment (e.g. VU108-, VU110-) and the top right superscripts
256 (G, B, A, O) in the sample IDs (e.g., G15M0029^G, G15M0021^B) refer to groundmass, biotite, amphibole and obsidian.

257 3.1.1 Groundmass $^{40}\text{Ar}/^{39}\text{Ar}$ plateau and/or isochron ages

258 All groundmass samples yielding $^{40}\text{Ar}/^{39}\text{Ar}$ plateau and isochron ages with more than 50% $^{39}\text{Ar}_k$ and less than 2.5 MSWD
259 included in their age spectrum are shown in Figure 4 and reported in Table 2. The $^{40}\text{Ar}/^{36}\text{Ar}$ isochron intercepts do not deviate
260 from atmospheric argon at the 2-sigma level, unless stated otherwise (Table 3). Sample G15M0016 was collected from a dyke
261 at Kleftiko in the southwest of Milos (Figure 2). Three incremental heating experiments were performed on the groundmass
262 of this sample (Figure 5A). The first experiment (VU108-Z8a) produced a weighted mean age of $2.71 \pm 0.02 \text{ Ma}$ (MSWD
263 2.31; $^{39}\text{Ar}_k$ 79.6%; inverse isochron age $2.65 \pm 0.10 \text{ Ma}$). The other two, VU108-Z8a_4 and VU108-Z8b_1, have plateau ages
264 of $2.61 \pm 0.03 \text{ Ma}$ (MSWD 0.93; $^{39}\text{Ar}_k$ 57.4%; inverse isochron age $2.69 \pm 0.10 \text{ Ma}$) and $2.67 \pm 0.01 \text{ Ma}$ (MSWD 1.50; $^{39}\text{Ar}_k$
265 65.57%; inverse isochron age $2.55 \pm 0.05 \text{ Ma}$), respectively. The three experiments are remarkably similar. Although the
266 amount of radiogenic ^{40}Ar is low (<20%), a combined age of $2.66 \pm 0.01 \text{ Ma}$ is considered to be the best estimate with a
267 relatively high MSWD value (2.51).



268
269 **Figure 5. Groundmass $^{40}\text{Ar}/^{39}\text{Ar}$ plateau ages for samples G15M0016 (A), G15M0032B (B), G15M0019 (C) and G15M0020 (D).**
270 **The Mavro Vouni dome (A), Dhemeneghaki volcano (B) and Kontaro dacitic dome (C, D) are located in respectively the south-**
271 **western, north-eastern and eastern parts of Milos VF (see Fig. 2). Final age calculation is reported with 1σ errors. See the**
272 **individual steps of sample G15M0016, G15M0019 and G15M0029 in supplementary material II.**

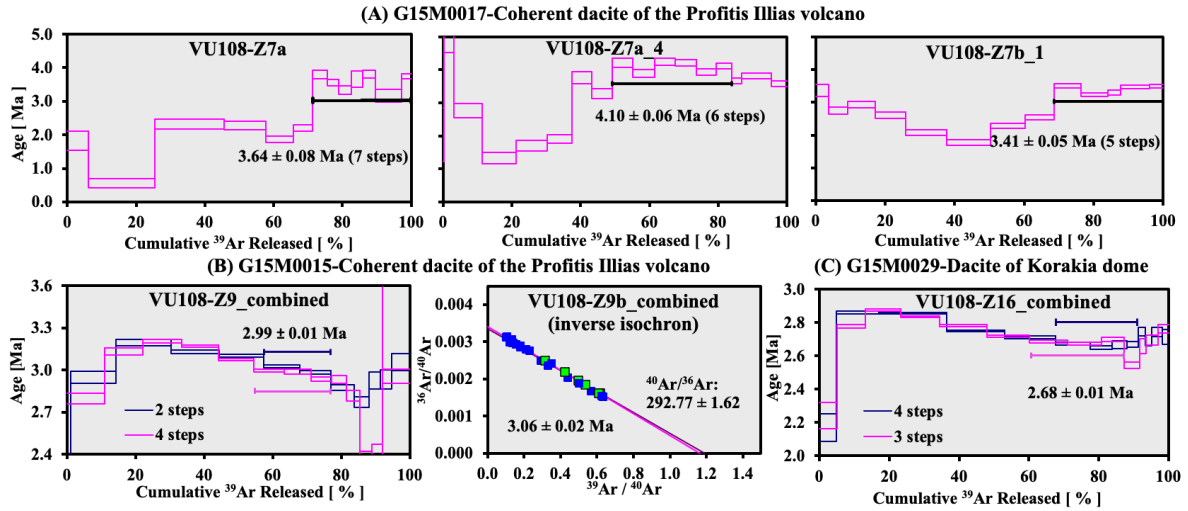
273 Two lava samples, G15M0019 and G15M0020, were collected from Kontaro in north-eastern Milos (Figure 2). Three replicate
274 incremental heating step experiments on groundmass from sample G15M0019 (VU108-Z6a_4; VU108-Z6a_5 and VU108-
275 Z6b_1, Figure 5B) were performed that are not reproducible. Their plateau ages range from 1.55 Ma to 1.62 Ma with relatively
276 high MSWD (3.8-4.5), 56-95% of the total $^{39}\text{Ar}_K$, 34-53% of radiogenic ^{40}Ar , 0.88-1.02 of K/Ca and an atmospheric isochron
277 intercept of 297-315. We consider the isochron age from the last experiment (VU108-Z6b_1) as the reliable age (1.48 ± 0.02
278 Ma, MSWD 0.44) because its MSWD value is the only one smaller than 2.5 in this experiment, and therefore the best estimate
279 for the eruption age. Three replicate incremental heating step experiments on groundmass from sample G15M0020 (VU108-
280 Z5a_5; VU108-Z5b_1 and VU108-Z5b_2, Figure 5C) were analysed. These experiments are similar at the lower temperature
281 heating steps. They produced statistically meaningful plateau ages ranging from 1.52-1.56 Ma with 41-62% of the total $^{39}\text{Ar}_K$,
282 18-48% of radiogenic ^{40}Ar , 1.51-1.73 of K/Ca and an atmospheric isochron intercept of 295-300. Their combined weighted
283 mean age is 1.54 ± 0.01 Ma (MSWD 3.06; $^{39}\text{Ar}_K$ 57.32%) with 25.31% of $^{40}\text{Ar}^*$.

284 Sample G15M0032B (obsidian) was collected from a pumice cone volcano at Demeneghaki (Figure 2). One incremental
285 heating experiment on this sample (VU108-Z18, Figure 5D) yielded a plateau age of 1.825 ± 0.002 Ma (MSWD 0.91; $^{39}\text{Ar}_K$
286 98.6%). The $^{40}\text{Ar}^*$ is 93.86%. The inverse isochron age is identical to the weighted mean plateau age of 1.825 ± 0.002 Ma.
287 The age of 1.825 ± 0.002 Ma is considered the best estimate for the eruption age of the Demeneghaki obsidian.

288 3.1.2 Groundmass $^{40}\text{Ar}/^{39}\text{Ar}$ plateau and/or isochron ages (25-40% $^{39}\text{Ar}_K$ released)

289 The results shown in Figure 5 did not yield weighted mean plateau ages according to standard criteria including $^{39}\text{Ar}_K > 50\%$,
290 but still provide some useful age information. Sample G15M0017 was collected from a cryptodome of the Profitis Illias
291 volcano of southwestern Milos (Figure 2). Three replicate incremental heating experiments, VU108-Z7a, VU108-Z7a_4 and
292 VU108-Z7b_1, have been performed on this sample which resulted in disturbed age spectra (Figure 6A). The consecutive
293 lower temperature steps of all experiments define ages of < 2.5 Ma, which is much younger than the ages of the submarine
294 pyroclastic products of the lower series at Kleftiko and/or Profitis Illias (3.0-3.5 Ma, Fytikas et al., 1986 and Stewart and
295 McPhie, 2006). At the consecutive higher temperature heating steps, these experiments yielded 3.64 ± 0.08 Ma ($^{40}\text{Ar}/^{36}\text{Ar}$
296 293.87 ± 4.77 ; VU108-Z7a), 4.10 ± 0.06 Ma ($^{40}\text{Ar}/^{36}\text{Ar}$ 298.44 ± 15.51 ; VU108-Z7a_4) and 3.41 ± 0.05 Ma ($^{40}\text{Ar}/^{36}\text{Ar}$ 295.97
297 ± 7.34 ; VU108-Z7b_1). The total fusion and inverse isochron ages of the three experiments gave large ranges of 2.25-3.23 and
298 3.68-4.14 Ma, respectively, and none of these high temperature heating steps produced a statistical plateau (all MSWD > 2.0).

299 The amount of radiogenic ^{40}Ar of both the $^{40}\text{Ar}/^{39}\text{Ar}$ result from our sample and the K-Ar age data from previous studies
 300 (Fytikas et al., 1986) is rather low (<15%) for a sample of this age based on our laboratory experience. Therefore, the estimated
 301 age range for the oldest volcanic products of the Milos VF should be confirmed by other dating techniques.



302
 303 **Figure 6. Groundmass $^{40}\text{Ar}/^{39}\text{Ar}$ plateau or inverse isochron ages for samples G15M0017 (A), G15M0015 (B) and G15M0029 (C).**
 304 **Individual steps and final age calculation are reported with 1σ errors. The Profitis Ilias volcano (A, B) and dacitic Korakia dome**
 305 **(C) are located in the south-western and north-eastern parts of Milos VF, respectively (Fig. 2). See the individual steps of sample**
 306 **G15M0015 and G15M0029 in supplementary material II.**

307 Sample G15M0015 is also a cryptodome breccia from Profitis Ilias (Figure 2). Two replicate incremental step heating
 308 experiments were performed on the groundmass of this sample (VU108-Z9a and VU108-Z9b_1, Figure 6B). Experiment
 309 VU108-Z9a groundmass shows a disturbing age spectrum and ages increase from ~3 Ma in the initial heating steps to ~3.2
 310 Ma, followed by a decrease to ~3 Ma in the high temperature heating steps. The consecutive heating steps only exist at the
 311 lower temperature steps yielding a “plateau” of 3.12 ± 0.02 Ma (MSWD 9.07). Due to the excess argon ($^{40}\text{Ar}/^{36}\text{Ar}$ $304.19 \pm$
 312 1.25 comprising 43.07% of the released $^{39}\text{Ar}_K$), the inverse isochron of 3.06 ± 0.02 Ma (MSWD 0.01) is more reliable for this
 313 analysis. The inverse isochron age of the second groundmass (VU108-Z9b_1) is identical at 3.04 ± 0.02 Ma (MSWD 1.14;
 314 $^{39}\text{Ar}_K$ 27.00%) and $^{40}\text{Ar}/^{36}\text{Ar}$ of 293.83 ± 1.38 obtained at high temperature steps. The two experiments are remarkably similar.
 315 Although the sample does not formally fulfil the definition of a plateau age comprising >50% $^{39}\text{Ar}_K$ released, a combined age
 316 of 3.06 ± 0.02 Ma (MSWD 1.14; $^{39}\text{Ar}_K$ 22.79%, $^{40}\text{Ar}^*$ 41.77%) most likely represents the eruption age. This $^{40}\text{Ar}/^{36}\text{Ar}$ age is
 317 consistent with the K-Ar age from the same lithology of 3.08 ± 0.08 Ma (Fytikas et al. 1986).

318 Sample G15M0029 is an andesite collected from Korakia in the northeast of Milos (Figure 2). Two incremental heating
 319 experiments (VU108-Z16a and VU108-Z16b_1, Figure 6C) were performed on this sample. The two experiments are
 320 remarkably similar and show a decreasing age from ~2.85 Ma at the lower temperature heating steps to 2.65 Ma at the higher
 321 temperatures. The higher temperature heating steps of both experiments yielded weighted mean plateau ages of 2.67 ± 0.01
 322 Ma (MSWD 0.96; $^{39}\text{Ar}_K$ 23.61%, $^{40}\text{Ar}^*$ 56.34%; inverse isochron age 2.68 ± 0.02 Ma) and 2.69 ± 0.01 Ma (MSWD 1.32;
 323 $^{39}\text{Ar}_K$ 27.08%, $^{40}\text{Ar}^*$ 55.78%; inverse isochron age 2.67 ± 0.03 Ma). The isochron intercepts for both experiments are
 324 atmospheric. The combined age of 2.68 ± 0.01 Ma should be considered with caution due to the rather low amount of released
 325 ^{39}Ar (23-28%).

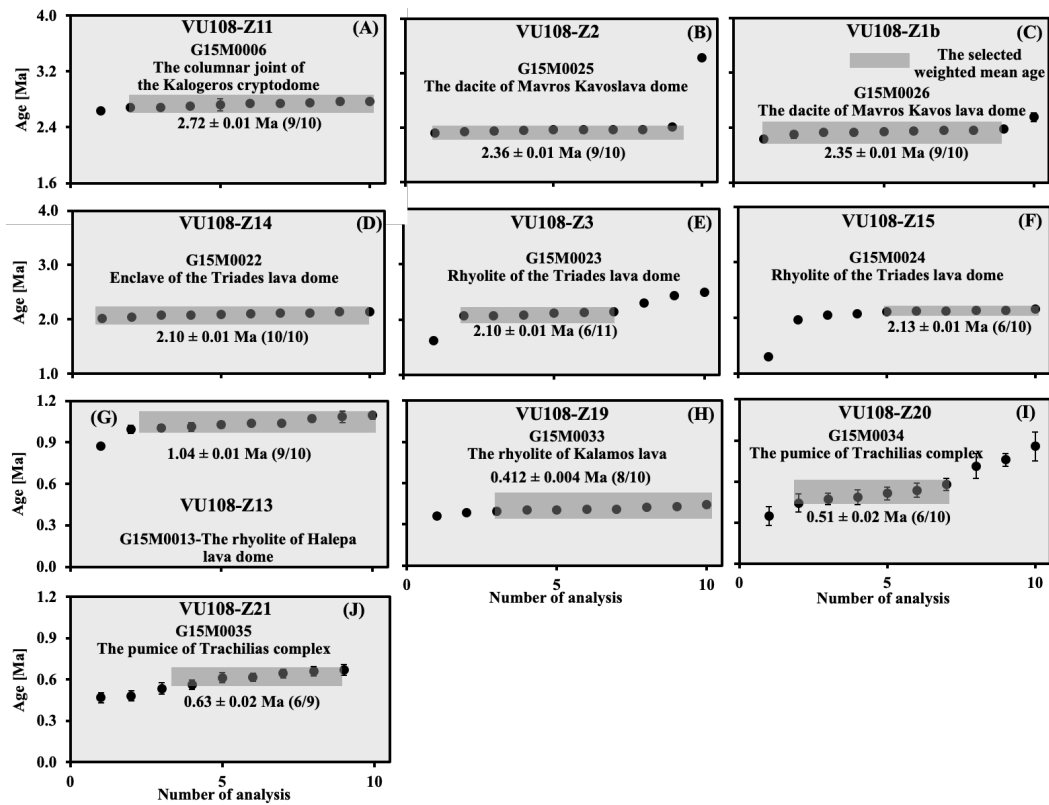


Figure 7. Biotite $^{40}\text{Ar}/^{39}\text{Ar}$ total fusion ages for samples G15M0006 (A) and G15M0025-26(B, C), G15M0022-24 (D-F), G15M0013 (G) and G15M0033-35 (H-J). Data outside the shaded area are not included in the weighted mean. Individual steps and final age calculation are reported with 1σ errors. The Kalogeros cryptodome and Mavros Kavos lava dome are located in the north-eastern and south-western parts of Milos VF, respectively, and Triades lava dome, Halepa lava dome, Trachilias complex and the Kalamos lava are situated in the southern, northern and south-eastern parts of Milos VF, respectively (see Fig. 2).

3.1.3 Single biotite grain $^{40}\text{Ar}/^{39}\text{Ar}$ fusion and/or isochron ages

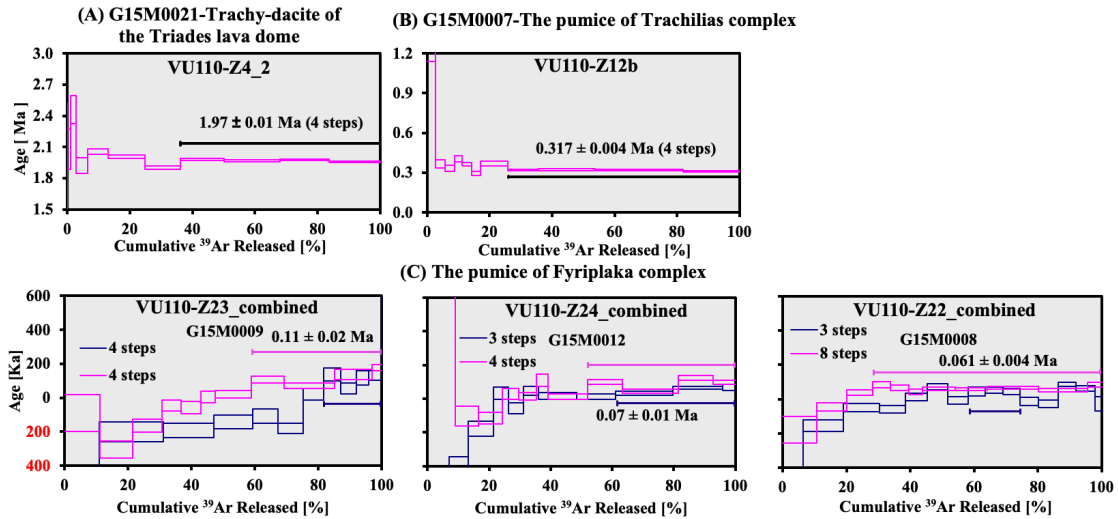
Results of nine single fusion experiments are given in Figure 7. Nine or ten replicate single fusion experiments were conducted on 5-10 grains biotite per fusion. Sample G15M0006 is from dacite with columnar joints from the Kalogeros cryptodome in the northeast of Milos (VU108-Z11, Figure 7A). The sample shows a weighted mean age of 2.72 ± 0.01 Ma for 9 out of 10 total fusion experiments (MSWD 1.95; 9/10) with an average 47.9% of radiogenic ^{40}Ar . The inverse isochron age is 2.62 ± 0.04 Ma (MSWD 0.99). Note that excess argon ($^{40}\text{Ar}/^{36}\text{Ar}$ 310.2 ± 4.0) is present. Hence the inverse isochron age is younger compared to the weighted mean age. The isochron age of 2.62 ± 0.04 Ma is considered as the best estimate for the emplacement age.

Sample G15M0025 was collected from the Mavros Kavos lava dome located in the west of Milos (Figure 2). The biotite of this sample (VU108-Z2, Figure 7B) shows a weighted mean age of 2.36 ± 0.01 Ma (MSWD 0.70; 9/10; $^{40}\text{Ar}^*$ 37.60%, inverse isochron age 2.34 ± 0.04 Ma) with an $^{40}\text{Ar}/^{36}\text{Ar}$ intercept of 300.6 ± 3.5 . The age of 2.36 ± 0.01 Ma is considered the best eruption age estimate for this sample.

Sample G15M0023 and G15M0024 are from the Triades lava dome northeast of Milos (Figure 2). A mafic enclave G15M0022 (host rock G15M0021) was collected from a lava near Cape Vani (Figure 2). The total fusion experiments of the biotites show that their initial $^{40}\text{Ar}/^{36}\text{Ar}$ estimates overlap with air (296-300). The total fusion ages gave the best estimates for their eruption ages of 2.10-2.13 Ma using 22 out of 31 fusions with a range of radiogenic ^{40}Ar between 30-36% (Figure 7B).

Sample G15M0013 is from the rhyolitic Halepa lava dome in the south of Milos (Figure 2). The total fusion experiment (VU108-Z13, Figure 7C) on biotite of this sample produced a weighted mean age of 1.04 ± 0.01 Ma (MSWD 1.62; 9/10, $^{40}\text{Ar}^*$ 26.3%; inverse isochron age 1.02 ± 0.04 Ma) with an initial $^{40}\text{Ar}/^{36}\text{Ar}$ estimate of 299.8 ± 4.1 . The best estimate for the eruption age of the Halepa rhyolite is 1.04 ± 0.01 Ma.

352 Sample G15M0034 and G15M0035 were collected from a lava dome located southeast of the Trachilas cone (Figure 2). Nine
 353 total fusion experiments (VU108-Z21, Figure 7C) were performed on biotite of sample G15M0035 and yielded the age of 0.63 ± 0.02 Ma (MSWD 1.26; 6/9; $^{40}\text{Ar}^*$ 4.9%; inverse isochron age 0.77 ± 0.13 Ma). The atmospheric isochron intercept overlaps
 354 with air at 2-sigma (296.4 ± 1.7). The 4.9% of radiogenic ^{40}Ar is so low that we should consider the age of 0.63 ± 0.02 Ma
 355 with caution. For biotite of sample G15M0034 (VU108-Z20, Figure 7C) one total fusion experiment produced a weighted
 356 mean age of 0.51 ± 0.02 Ma (MSWD 0.95; 6/10; $^{40}\text{Ar}^*$ 3.5%; inverse isochron age 0.61 ± 0.08 Ma) with an atmospheric
 357 isochron intercept. The age of 0.51 ± 0.02 Ma also needs to be considered as possibly suspect due to the low amount of
 358 radiogenic ^{40}Ar .
 359



360
 361 **Figure 8. Biotite $^{40}\text{Ar}/^{39}\text{Ar}$ plateau ages for samples G15M0021 (A), G15M0007 (B), and G15M0009 (VU110-Z23_combined),**
 362 **G15M0012 (VU110-Z24_combined) and G15M0008 (VU110-Z22_combined) (C). The numbers in red represent negative ages.**
 363 **Individual steps and final age calculation are reported with 1σ errors. The Triades lava dome, Trachilias and Fyriplaka complexes**
 364 **are located in the north-western, northern and south-eastern parts of Milos VF, respectively (see Fig. 2). See the individual steps of**
 365 **sample G15M0021, G15M0007, G15M0009, G15M0012 and G15M0008 in supplementary material II.**

366 Sample G15M0033 was collected from the Kalamos lava along the coast of the southwest of the Fyriplaka rhyolitic complex
 367 (Figure 2). Biotite of this sample (VU108-Z19, Figure 7C) yielded 0.412 ± 0.004 Ma (MSWD 1.10; 8/10; inverse isochron
 368 age 0.39 ± 0.02 Ma) with $\sim 22.2\%$ of radiogenic ^{40}Ar which is considered as the eruption age for the Kalamos lava.

369 3.1.4 Multiple biotite grain $^{40}\text{Ar}/^{39}\text{Ar}$ incremental heating plateau and/or isochron ages

370 Figure 8 displays the biotite $^{40}\text{Ar}/^{39}\text{Ar}$ ages measured by the incremental heating steps method. Sample G15M0021 is the host
 371 lava of mafic enclave G15M0022. Twelve replicate total fusion experiments on its biotite (VU110-Z4, Table 3) produced an
 372 age of 2.48 ± 0.04 Ma (MSWD 1.49; 4/12, $^{40}\text{Ar}^*$ 36.09%; inverse isochron age 3.44 ± 0.46 Ma). Although this suggests a
 373 correct age, the large analytical error of each fusion (>0.3 Ma on average) and poor reproducibility (4/12) of this experiment
 374 probably results in an unreliable age. Therefore, two more incremental heating experiments were performed on this sample
 375 (VU110-Z4_2 and VU110-Z4_2b, Figure 8A), that gave an age of 1.97 ± 0.01 Ma (MSWD 1.66; $^{39}\text{Ar}_K$ 63.8%, $^{40}\text{Ar}^*$ 54.7%;
 376 inverse isochron age 1.97 ± 0.03 Ma) and 2.01 ± 0.01 Ma (MSWD 6.76; $^{39}\text{Ar}_K$ 75.39%, $^{40}\text{Ar}^*$ 57.84%; inverse isochron age
 377 2.04 ± 0.05 Ma), respectively. The scatter in the latter is too high to define a reliable plateau age and the first incremental
 378 heating experiment is considered as the best estimate of the eruption age of this sample.

379 Sample G15M0007 was collected from the rhyolitic Trachilias complex in the north of Milos (Figure 2). Twenty-two total
 380 fusion (VU110-Z12, Table 3) and two incremental heating experiments (VU110-Z12a and 12b, Figure 8B) were performed
 381 on biotite of this sample. The total fusion experiments did not result in a reliable age due to the large errors of single steps (\pm
 382 0.19 Ma on average) and the rather low amount of radiogenic ^{40}Ar (9.1%). On the other hand, the first incremental heating
 383 experiment produced a plateau age of 0.30 ± 0.01 Ma (MSWD 4.61; $^{39}\text{Ar}_K$ 56.60%; inverse isochron age 0.28 ± 0.05 Ma)
 384 including 14.51% of radiogenic ^{40}Ar . The second incremental heating experiment yielded a plateau of 0.317 ± 0.004 Ma

385 (MSWD 1.29; $^{39}\text{Ar}_K$ 74.05%; inverse isochron age 0.31 ± 0.03 Ma) with a higher amount of radiogenic ^{40}Ar (18.30%). The
 386 isochron intercepts of both incremental heating experiments are atmospheric. The second experiment is the best estimate for
 387 the eruption age, since it contained the largest amount of radiogenic ^{40}Ar and has a better reproducibility of single heating
 388 steps.

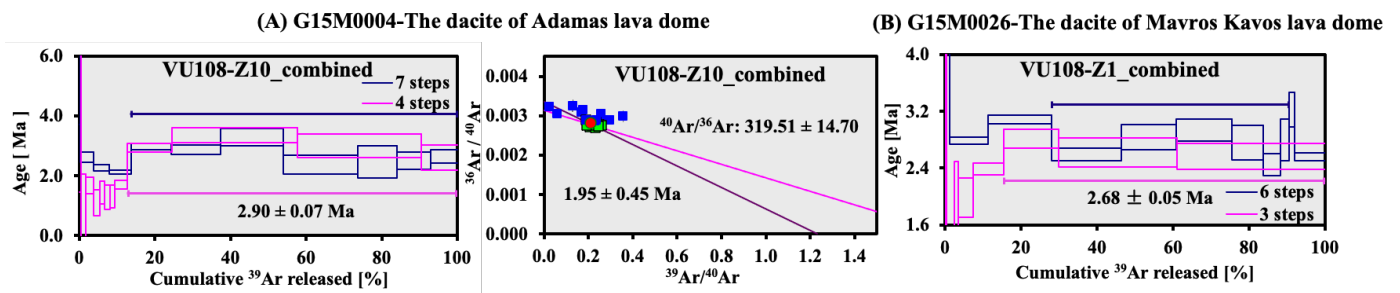
389 Three pumice clasts (G15M0008-9 and G15M0012) were sampled from different layers of the Fyriplaka complex (Figure 2).
 390 The first incremental step heating experiment on biotite from sample G15M0009 (VU110-Z23a, Figure 8C) gave negative
 391 ages at the lower temperature heating steps. Four consecutive higher temperature heating steps seem to define a “plateau” of
 392 0.11 ± 0.02 Ma (MSWD 1.37) only using 18.33% of the total $^{39}\text{Ar}_K$ with 1.65% of radiogenic ^{40}Ar . The second experiment
 393 (VU110-Z23b) also yielded a “plateau” of 0.11 ± 0.03 Ma (MSWD 6.77) at higher temperature heating steps including 41.05%
 394 of the total $^{39}\text{Ar}_K$ and 3.13% of radiogenic ^{40}Ar . The significantly larger error of the isochron age may be due to the clustering
 395 of data close to zero on the y-axis. The two experiments (VU110-Z23a and Z23b) are comparable. The combined age of 0.11
 396 ± 0.02 (MSWD 3.5) is consistent with the age of 0.09-0.14 Ma from Fytikas et al. (1986). Although only 29.50% of the released
 397 $^{39}\text{Ar}_K$ was used for this sample, this age still probably represents the eruption age of this layer in the Fyriplaka complex.

398 For biotite of sample G15M0012, both incremental step heating experiments are comparable. Both of them yielded plateau
 399 ages of 0.05 ± 0.01 Ma (VU110-Z24a; MSWD 3.09; $^{39}\text{Ar}_K$ 38.89%, $^{40}\text{Ar}^*$ 2.89%; inverse isochron age 0.14 ± 0.03 Ma) and
 400 0.09 ± 0.02 Ma (VU110-Z24b; MSWD 8.16; $^{39}\text{Ar}_K$ 48.04%, $^{40}\text{Ar}^*$ 4.59%; inverse isochron age 0.09 ± 0.05 Ma) at higher
 401 temperature heating steps (Figure 8C). The clustering of data points of experiment VU110-Z24a could result in the lower
 402 initial estimate of $^{40}\text{Ar}/^{36}\text{Ar}$ (285.98 ± 4.76). However, the combined age of 0.07 ± 0.01 Ma, using 43.53% of the total $^{39}\text{Ar}_K$
 403 with an atmospheric isochron intercept (295.67 ± 7.39), could be the representative age of eruption.

404 Biotite of sample G15M0008 did not result in a reliable plateau in the first incremental step heating experiment (VU110-Z22a,
 405 Figure 8C) but shows a very disturbed age spectrum. The second experiment (VU110-Z22b) yielded 0.062 ± 0.003 Ma (MSWD
 406 0.91) using 71.81% of the total $^{39}\text{Ar}_K$ with 2.69% of radiogenic ^{40}Ar as the best estimate of the eruption age.

407 3.1.5 Multiple amphibole grain $^{40}\text{Ar}/^{39}\text{Ar}$ multi-grain incremental heating plateau and/or isochron ages

408 There are only two amphibole samples that yielded $^{40}\text{Ar}/^{36}\text{Ar}$ plateau and/or isochron ages (Figure 9A and B). Sample
 409 G15M0004 was collected from the pyroclastic series of Adamas from the PSLD (Fytikas et al., 1986), to the north of Bombarda
 410 (Figure 2). Two replicate heating experiments of G15M0004 amphibole (VU108-Z10_1 and VU108-Z10_2) were performed



411
 412 **Figure 9. Amphibole $^{40}\text{Ar}/^{39}\text{Ar}$ plateau or inverse isochron ages for samples G15M0004 (A) and G15M0026 (B). Final age**
 413 **calculation is reported with 1σ errors. The Adamas and Mavros Kavos lava domes are located in the northern and south-western**
 414 **parts of Milos VF, respectively (see Fig. 2). See the individual steps of sample G15M0004 and G15M0026 in supplementary**
 415 **material II.**

416 yielding 2.99 ± 0.11 Ma (MSWD 1.00; $^{39}\text{Ar}_K$ 87.31%, $^{40}\text{Ar}^*$ 16.36%; inverse isochron age 7.89 ± 2.46 Ma) and 2.86 ± 0.09
 417 Ma (MSWD 1.50; $^{39}\text{Ar}_K$ 86.18%, $^{40}\text{Ar}^*$ 17.58%; inverse isochron age 0.70 ± 0.29 Ma). The variable atmospheric isochron
 418 intercept of both experiments ($^{40}\text{Ar}/^{36}\text{Ar}$ 202.39 ± 48.47 and 348.91 ± 27.33) is due to the clustering of the data points. Note
 419 that also the amount of radiogenic ^{40}Ar is rather low (~17%). The two experiments are remarkably similar. A combined inverse
 420 isochron age of 1.95 ± 0.45 Ma (MSWD 1.17; $^{40}\text{Ar}/^{36}\text{Ar}$ 319.51 ± 14.70) is considered the best estimate, but ideally this age
 421 should be checked by other techniques.

422 Table 2. Incremental heating $^{40}\text{Ar}/^{39}\text{Ar}$ results of the Milos volcanic field.

Volcanic Unit	Sample -ID	Irr-ID	Latitude	Age $\pm 1\sigma$ (Ma)	MS WD	$^{39}\text{Ar}_K$ (%)	n/ntotal	$^{40}\text{Ar}^*$ (%)	K/Ca $\pm 1\sigma$	Inverse isochron age (Ma)	$^{40}\text{Ar}/^{36}\text{Ar} \pm 1\sigma$	MS WD
Fyriplaka Complex	G15 M00 08 ^B	VU110-Z22a	36.67 29 N	0.05 \pm 0.01	0.04	16.24	3/15	1.20	60.9 \pm 10.6	0.05 \pm 0.10	298.08 \pm 8.77	0.08
		VU110-Z22b	24.46 70 E	0.062 \pm 0.003	0.91	71.81	8/11	2.69	57.3 \pm 8.4	0.06 \pm 0.02	299.39 \pm 3.66	1.09
		Combined (Z22)	70 E	0.061 \pm 0.004	0.82	41.37	11/26	2.29	58.0 \pm 6.3	0.07 \pm 0.01	296.78 \pm 1.78	0.83
	G15 M00 12 ^B	VU110-Z24a	36.67 95 N	0.05 \pm 0.01	3.09	38.89	3/11	2.89	40.0 \pm 6.0	0.14 \pm 0.03	285.98 \pm 4.76	0.07
		VU110-Z24b	24.48 28 E	0.09 \pm 0.02	8.16	48.04	4/11	4.59	30.1 \pm 7.1	0.09 \pm 0.05	297.46 \pm 10.29	12.78
		Combined(Z24)	28 E	0.07 \pm 0.01	7.44	43.53	7/22	3.86	32.3 \pm 5.0	0.09 \pm 0.03	295.67 \pm 7.39	9.02
	G15 M00 09 ^B	VU110-Z23a	36.67 16 N	0.11 \pm 0.02	1.37	18.33	4/12	1.65	45.4 \pm 7.3	0.76 \pm 0.30	268.52 \pm 17.08	0.90
		VU110-Z23b	24.48 91 E	0.11 \pm 0.03	6.77	41.05	4/11	3.13	19.4 \pm 3.7	0.29 \pm 0.14	285.17 \pm 15.80	8.09
		Combined (Z23)	91 E	0.11 \pm 0.02	3.50	29.50	8/21	2.39	19.7 \pm 2.6	0.15 \pm 0.05	295.78 \pm 4.34	4.04
Trachilas Complex	G15 M00 07 ^B	VU110-Z12a	36.76 71 N	0.30 \pm 0.01	4.61	56.50	8/16	14.51	38.3 \pm 2.4	0.28 \pm 0.05	301.42 \pm 9.01	5.47
		VU110-Z12b	24.41 24 E	0.317 \pm 0.004	1.29	74.05	4/11	18.30	32.0 \pm 2.5	0.31 \pm 0.03	299.52 \pm 6.40	2.04
		Combined (Z12)	24 E	0.31 \pm 0.01	5.57	65.27	12/27	15.77	33.1 \pm 1.6	0.34 \pm 0.03	293.05 \pm 5.50	5.84
Kontaro dome	G15 M00 20 ^G	VU108-Z5a_5	36.72 34 N	1.52 \pm 0.01	1.06	61.82	8/12	18.30	1.51 \pm 0.05	1.49 \pm 0.02	300.03 \pm 0.86	0.95
		VU108-Z5b_1	24.39 52 E	1.56 \pm 0.01	1.94	41.54	3/10	47.94	1.73 \pm 0.06	1.58 \pm 0.02	294.97 \pm 3.74	2.17
		VU108-Z5b_2	24.39 52 E	1.52 \pm 0.01	1.73	62.45	5/10	22.95	1.56 \pm 0.08	1.53 \pm 0.02	298.12 \pm 0.89	2.34
		Combined (Z5)	52 E	1.54 \pm 0.01	3.06	57.32	16/32	25.31	1.58 \pm 0.04	1.55 \pm 0.01	297.41 \pm 0.57	2.82
	G15 M00 19 ^G	VU108-Z6a_4	36.72 11 N	1.62 \pm 0.01	3.80	89.75	9/11	34.28	0.91 \pm 0.05	1.62 \pm 0.02	297.66 \pm 1.36	4.40
		VU108-Z6a_5	24.39 50 E	1.55 \pm 0.01	4.50	95.41	10/12	35.26	0.88 \pm 0.06	1.55 \pm 0.01	298.73 \pm 1.29	5.40
		VU108-Z6b_1	24.39 50 E	1.56 \pm 0.01	4.05	56.64	4/10	53.19	1.02 \pm 0.01	1.48 \pm 0.02	315.46 \pm 5.20	0.44
Combined (Z6)	50 E	1.55 \pm 0.01	32.15	80.97	27/45	38.78	0.93 \pm 0.04	1.53 \pm 0.02	300.60 \pm 2.27	34.25		
Dheme-neghaki volcano	G15 M00 32B ^O	VU108-Z18	36.70 84 N 24.53 24 E	1.825 \pm 0.002	0.91	98.64	12/13	93.86	1.83 \pm 0.04	1.825 \pm 0.003	301.52 \pm 3.34	0.93
Triades lava dome	G15 M00 21 ^B	VU110-Z4_2	36.74 02 N	1.97 \pm 0.01	1.66	63.83	4/12	54.72	107.55 \pm 20.64	1.97 \pm 0.03	299.16 \pm 5.36	2.56
		VU110-Z4_2b	24.33 97 E	2.01 \pm 0.01	6.76	75.39	6/16	57.84	54.43 \pm 8.29	2.04 \pm 0.05	293.08 \pm 10.44	8.15
		Combined (Z4)	97 E	1.99 \pm 0.01	9.08	69.12	10/28	56.59	73.52 \pm 6.46	2.00 \pm 0.04	295.64 \pm 7.89	10.30
Adamas lava dome	G15 M00 04 ^A	VU108-Z10_1	36.72 82 N	2.99 \pm 0.11	1.00	87.31	4/12	16.36	0.030 \pm 0.002	7.89 \pm 2.46	202.39 \pm 48.47	0.01
		VU108-Z10_2	24.43 15 E	2.86 \pm 0.09	1.50	86.18	7/11	17.58	0.029 \pm 0.002	0.70 \pm 0.29	348.91 \pm 27.33	1.00
		Combined (Z10)	15 E	2.90 \pm 0.07	1.31	86.74	11/23	17.13	0.029 \pm 0.001	1.95 \pm 0.45	319.51 \pm 14.70	1.17
The dyke of Mavro Vouni lava dome	G15 M00 16 ^G	VU108-Z8a	36.66 68 N	2.71 \pm 0.02	2.31	79.64	8/12	16.57	0.24 \pm 0.05	2.65 \pm 0.10	299.84 \pm 2.32	2.92
		VU108-Z8a_4	24.33 98 E	2.61 \pm 0.03	0.93	57.41	7/12	16.86	0.12 \pm 0.07	2.69 \pm 0.10	296.44 \pm 2.49	0.69
		VU108-Z8b_1	24.33 98 E	2.67 \pm 0.01	1.50	65.57	7/11	17.25	0.11 \pm 0.04	2.55 \pm 0.05	301.53 \pm 1.14	0.71
		Combined (Z8)	98 E	2.66 \pm 0.01	2.51	67.27	22/35	16.87	0.14 \pm 0.02	2.61 \pm 0.05	300.01 \pm 1.18	2.78
Korokia dome	G15 M00 29 ^G	VU108-Z16a	36.74 65 N	2.67 \pm 0.01	0.96	23.61	4/13	56.34	0.53 \pm 0.05	2.68 \pm 0.02	296.64 \pm 3.18	1.25
		VU108-Z16b_1	24.52 00 E	2.69 \pm 0.01	1.32	27.08	3/13	55.78	0.55 \pm 0.04	2.67 \pm 0.03	301.16 \pm 4.72	2.13
		Combined (Z16)	00 E	2.68 \pm 0.01	1.66	25.30	7/26	56.10	0.54 \pm 0.03	2.67 \pm 0.02	300.00 \pm 2.94	1.98
Coherent dacite of Profitis Ilias volcano	G15 M00 15 ^G	VU108-Z9a	36.66 29 N	3.12 \pm 0.02	9.07	43.07	3/12	42.73	1.31 \pm 0.05	3.06 \pm 0.02	304.19 \pm 1.25	0.01
		VU108-Z9b_1	24.35 96 E	2.98 \pm 0.02	4.53	27.00	4/14	39.35	0.98 \pm 0.06	3.04 \pm 0.02	293.83 \pm 1.38	1.14
		Combined (Z9)	96 E	2.99 \pm 0.02	5.54	22.79	6/26	41.77	1.00 \pm 0.04	3.06 \pm 0.02	292.77 \pm 1.62	1.90
Coherent dacite of Profitis Ilias volcano	G15 M00 17 ^G	VU108-Z7a	36.65 96 N	3.64 \pm 0.08	3.13	28.62	7/13	9.77	1.04 \pm 0.02	4.14 \pm 0.49	293.87 \pm 4.77	3.44
		VU108-Z7a_4	24.36 75 E	4.10 \pm 0.06	2.13	34.71	6/17	9.08	1.10 \pm 0.01	4.11 \pm 1.40	298.44 \pm 15.51	3.24
		VU108-Z7b_1	24.36 75 E	3.41 \pm 0.05	3.95	31.41	5/13	9.95	1.00 \pm 0.03	3.68 \pm 0.71	295.97 \pm 7.34	7.09
		Combined (Z7)	75 E	3.63 \pm 0.08	14.04	31.40	18/43	9.59	1.04 \pm 0.02	2.19 \pm 0.32	311.31 \pm 3.60	10.19

423 The age in bold is considered as the best estimate of the eruptive age.

424 The $^{40}\text{Ar}^*$ (%) is the average radiogenic ^{40}Ar of the analyses included in the weighted mean.425 The experiment was analyzed on biotite^B, obsidian^O, amphibole^A and groundmass^G of a sample.

426 The same steps were used for the calculation of isochron ages as used in the weighted mean ages.

Volcanic unit	Sample-ID	Irr-ID	Location	Age ± 1σ (Ma)	MS WD	³⁹ Ar _K (%)	n/ntotal	⁴⁰ Ar* (%)	K/Ca ± 1σ	Inverse isochron age (Ma)	⁴⁰ Ar/ ³⁶ Ar ± 1σ	MS WD
Fyriplaka complex	G15M0008 ^B	VU11 0-Z22	36.6729 N 24.4670 E	0.71 ± 0.06	0.41	25.78	8/23	8.67	17.5 ± 1.8	0.64 ± 0.20	302.75 ± 12.62	0.46
	G15M0012 ^B	VU11 0-Z24	36.6795 N 24.4828 E	1.12 ± 0.11	2.26	60.49	14/23	7.32	14.9 ± 0.8	0.26 ± 0.07	316.75 ± 19.49	2.29
	G15M0009 ^B	VU11 0-Z23	36.6716 N 24.4891 E	0.65 ± 0.07	1.16	79.91	19/23	5.87	12.0 ± 0.5	0.28 ± 0.07	309.57 ± 16.01	1.22
Trachilas complex	G15M0007 ^B	VU11 0-Z12	36.7671 N 24.4124 E	0.47 ± 0.05	0.75	72.65	15/22	9.09	14.8 ± 0.5	0.55 ± 0.12	293.95 ± 11.30	0.80
Kalamos lava	G15M0033 ^B	VU10 8-Z19	36.6662 N 24.4652 E	0.412 ± 0.004	1.10	77.24	8/10	22.22	20.5 ± 2.7	0.39 ± 0.02	303.32 ± 3.06	0.89
Trachilas complex	G15M0034 ^B	VU10 8-Z20	36.7550 N 24.4244 E	0.51 ± 0.02	0.95	56.92	6/10	3.53	13.7 ± 1.2	0.61 ± 0.08	296.45 ± 1.65	0.92
	G15M0035 ^B	VU10 8-Z21	36.7550 N 24.4244 E	0.63 ± 0.02	1.26	73.43	6/9	4.87	17.7 ± 1.1	0.77 ± 0.13	294.99 ± 3.17	1.42
Halepa lava dome	G15M0013 ^B	VU10 8-Z13	36.6716 N 24.4406 E	1.04 ± 0.01	1.62	82.40	9/10	26.30	*15.2 ± 0.2	1.02 ± 0.04	299.77 ± 4.06	0.00
Triades lava dome	G15M0021 ^B	VU11 0-Z4	36.7402 N 24.3397 E	2.48 ± 0.04	1.49	87.08	4/12	36.09	13.00±0.60	3.44 ± 0.46	228.58 ± 36.66	1.39
	G15M0022 ^B	VU10 8-Z14	36.7402 N 24.3397 E	2.10 ± 0.01	1.37	100.0 0	10/10	36.04	*11.7 ± 0.2	2.08 ± 0.06	299.44 ± 4.63	1.59
	G15M0023 ^B	VU10 8-Z3	36.7263 N 24.3420 E	2.10 ± 0.01	1.72	55.58	6/11	35.93	*76.1 ± 2.4	2.13 ± 0.06	296.12 ± 4.63	2.08
	G15M0024 ^B	VU10 8-Z15	36.7277 N 24.3415 E	2.13 ± 0.01	0.46	63.67	6/10	29.74	22.5 ± 3.2	2.09 ± 0.03	300.50 ± 1.58	0.23
Mavros Kavos lava dome	G15M0025 ^B	VU10 8-Z2	36.6876 N 24.3515 E	2.36 ± 0.01	0.70	84.62	9/10	37.62	43.2 ± 2.7	2.34 ± 0.04	300.57 ± 3.49	0.78
	G15M0026 ^B	VU10 8-Z1b	36.6848 N 24.3500 E	2.35 ± 0.01	1.36	95.23	9/10	38.56	12.8 ± 2.3	2.42 ± 0.04	292.01 ± 2.92	0.93
Kalegero scrypto-dome	G15M0006 ^B	VU10 8-Z11	36.7643 N 24.5157 E	2.72 ± 0.01	1.95	87.67	9/10	47.90	*28.3 ± 0.5	2.62 ± 0.04	310.21 ± 4.04	0.99

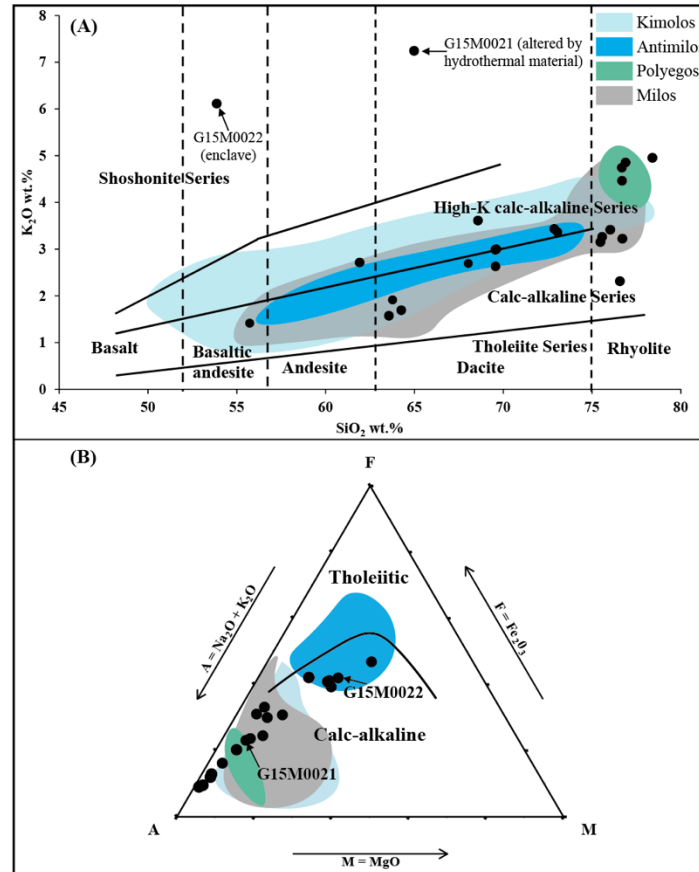
428 The age in bold is considered as the best estimate of the eruptive age.
429 The ⁴⁰Ar* (%) is the average radiogenic ⁴⁰Ar of the analyses included in the weighted mean.
430 *The K/Ca ratio is calibrated by removing the total fusion with excess ³⁷Ar (Ca) (fA>1).
431 ^BThe experiment was analyzed on biotite of the sample.
432 The same steps were used for the calculation of isochron ages as used in the weighted mean ages.

433 Sample G15M0026 is from the same location as sample G15M0025, which gives us the opportunity to compare the biotite age
434 with the amphibole age. One total fusion experiment on biotite (VU108-Z1b) yielded a weighted mean age of 2.35 ± 0.01 Ma
435 (MSWD 1.36; ⁴⁰Ar* 38.6%). The atmospheric isochron intercept is low (⁴⁰Ar/³⁶Ar 292.01 ± 2.92), the inverse isochron age of
436 2.42 ± 0.04 Ma (MSWD 0.93) is considered the best result from the biotite. Two incremental heating experiments for
437 amphibole (VU108-Z1b_1 and VU108-Z1b_2) gave plateau ages of 2.67-2.70 Ma which are much higher values than the
438 biotite inverse isochron ages (2.28-2.31 Ma). This result could be caused by the high ⁴⁰Ar/³⁶Ar isochron intercepts (>320) with
439 large uncertainties of ~29. Therefore, on the basis of the remarkable similarity of the two experiments, the combined inverse
440 isochron age of 2.31 ± 0.28 Ma (MSWD 0.93, ³⁹Ar_K 71.36%, ⁴⁰Ar* 34.97%) is considered as the best estimate from amphibole
441 which overlaps with the biotite age of 2.42 ± 0.03 Ma. This biotite age of 2.42 ± 0.03 Ma is considered to the best approximation
442 of the eruption age.

443 3.2 Major element results

444 Major-element results are given in Table 4. The major element compositions range from 54 to 78 wt.% SiO₂ (basaltic-andesite-
445 rhyolite to dacite-rhyolite, see Figure 10A). The most felsic samples (SiO₂>75 wt.%) belong to the Fyriplaka and Trachilas

446 complexes. Our data overlap with those of previous studies and display a similar range in SiO₂-K₂O (Francalanci and Zellmer,
 447 2019 and reference therein). The samples of Polyegos are similar to the Fyriplaka and Trachilas complexes, whereas the older
 448 Milos samples overlap with Kimolos and Antimilos (Fytikas et al., 1986, Francalanci et al., 2007).
 449 Although some samples of Antimilos are tholeiitic, all of the Milos volcanic units belong to the calc-alkaline and medium to
 450 high-K series (Figure 10B). A mafic inclusion, sample G15M0022, has high K₂O (6%), similar to sample G15M0021 (7.2
 451 wt.%). Both of them were collected from the Vani Cape area (Fig. 2). The SiO₂ wt.% versus our ⁴⁰Ar/³⁹Ar ages diagram (Figure
 452 11A) shows that there is a tendency of the volcanic units to become more felsic over time. In the diagram with K₂O/SiO₂
 453 versus age there is no significant change (Figure 11C).
 454



455
 456 **Figure 10. SiO₂ versus K₂O (A) and AFM (B) diagrams for the Milos volcanic field with data of this study as solid circles.**
 457 **Published data are represented by shaded fields (Francalanci and Zelmer, 2019 and reference therein). Fields for the tholeiite,**
 458 **calc-alkaline, high-K calc-alkaline and shoshonitic series are from Peccerillo and Taylor (1976). Vertical lines defining fields for**
 459 **basalt, basaltic-andesite, andesite, dacite and rhyolite are from Le Bas et al. (1986). The solid line dividing tholeiitic and calc-**
 460 **alkaline fields is from Irvine and Baragar (1971).**

461 **3.3 Variations of eruption volume with ages**

462 Figure 11a shows the cumulative volcanic output volume of the Milos VF over time. This diagram shows that the Milos VF
 463 can be separated into three periods: Periods I (~3.3-2.13 Ma) and III (1.48-0.00 Ma) are characterised by low volcanic output
 464 volumes, whereas Period II (2.13-1.48 Ma) shows a rapid increase in volcanic output volume. Period I and II are build up in
 465 submarine settings, whereas Period III is in a subaerial setting. The Milos VF was largely (~85% by volume) constructed in
 466 submarine before ~1.48 Ma (Period I and II) (Figure 11A). During Period III (1.48 Ma-present), only a small volume (~15%)
 467 of rhyolitic magma was added from different eruption vents. See the details of Period I-III in section 4.3.2.
 468

469 **Table 4. Major-element composition of volcanic samples from the Milos Volcanic Field.**

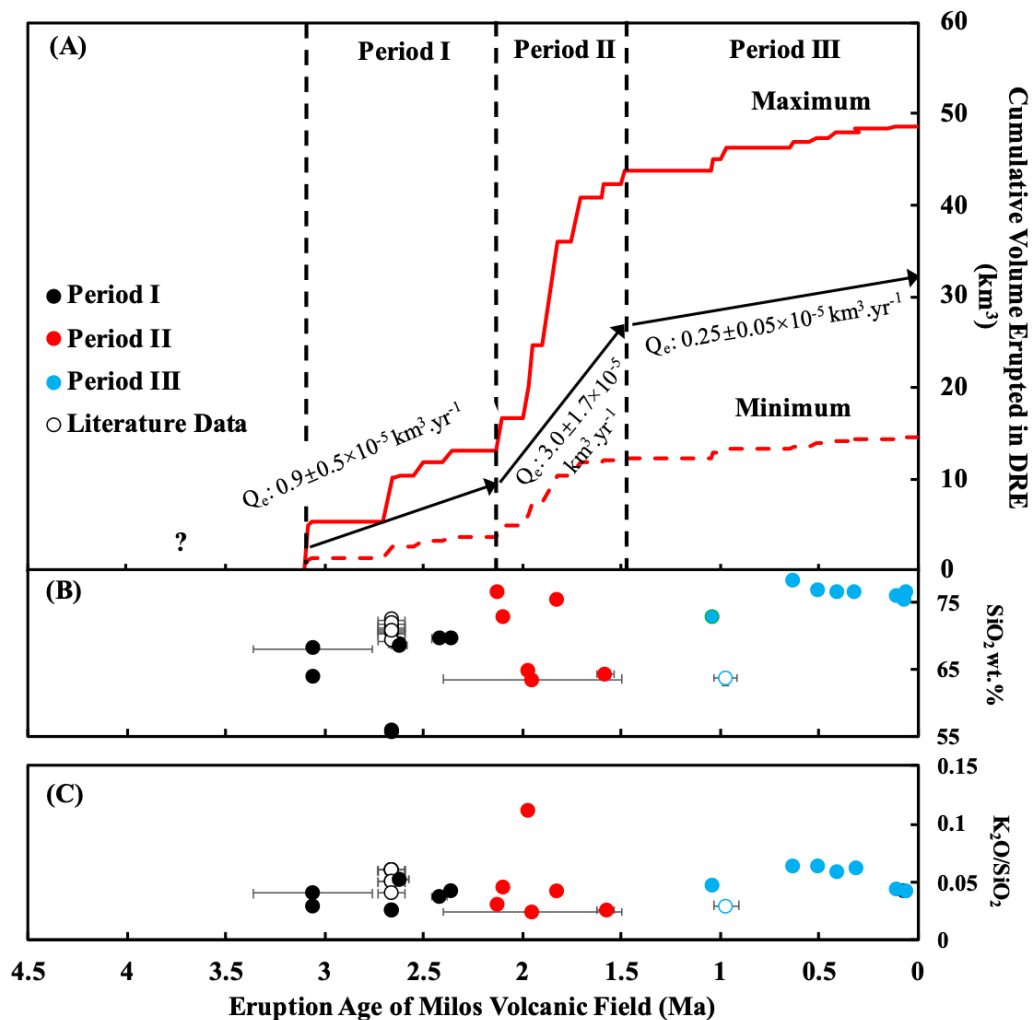
Sample-ID	G15M0 008	G15M0 012	G15M0 009	G15M0 007	G15M0 033	G15M0 034	G15M0 035	G15M0 013	G15M 0020	G15M 0019	G15M00 32B	G15M0 004
Rock Types	Pumice	Pumice	Pumice	Pumice	Pumice	Pumice	Pumice	Rhyolite	-	Dacite	Obsidian	Dacite
Period	III								II			
Major elements (wt.%)												
SiO ₂	76.71	75.47	76.02	76.68	76.68	76.89	78.40	72.87	-	64.26	75.57	63.56
TiO ₂	0.14	0.13	0.13	0.08	0.10	0.08	0.08	0.22	-	0.56	0.20	0.57
Al ₂ O ₃	12.96	12.77	12.91	12.60	12.86	12.64	12.93	14.11	-	16.08	13.32	16.09
Fe ₂ O ₃	1.11	1.08	1.04	0.85	0.88	0.84	0.85	1.95	-	5.33	1.46	5.70
MnO	0.06	0.06	0.06	0.08	0.09	0.09	0.09	0.07	-	0.11	0.06	0.11
MgO	0.22	0.22	0.23	0.11	0.18	0.11	0.11	0.51	-	2.42	0.33	2.81
CaO	1.27	1.27	1.19	0.75	0.85	0.74	0.76	2.23	-	5.33	1.71	6.01
Na ₂ O	4.04	4.12	3.99	3.58	3.71	3.50	3.49	3.73	-	3.60	3.95	3.49
K ₂ O	3.22	3.15	3.41	4.74	4.46	4.85	4.95	3.43	-	1.69	3.26	1.57
P ₂ O ₅	0.02	0.02	0.02	0.01	0.01	0.01	0.01	0.04	-	0.04	0.03	0.09
BaO	0.06	0.06	0.06	0.05	0.05	0.05	0.05	0.06	-	0.04	0.06	0.04
L.O.I.	0.16	0.35	0.16	0.17	0.14	0.33	0.06	0.13	-	0.09	0.07	0.04
Total	99.97	98.70	99.22	99.70	100.01	100.13	101.78	99.35	-	99.55	100.02	100.08

470

Sample-ID	G15M0 021	G15M0 022	G15M0 023	G15M0 024	G15M0 025	G15M0 026	G15M0 006	G15M0 016	G15M0 029	G15M0 015	G15M0 017
Rock Types	Trachy- dacite	Enclave	Dacite	Rhyolite	Dacite	Dacite	Dacite	Basaltic Andesite	Dacite	Dacite	Dacite
Period	II						I				
Major elements (wt.%)											
SiO ₂	64.98	53.87	73.05	76.57	69.56	69.57	68.58	55.72	61.91	63.77	68.03
TiO ₂	0.35	0.60	0.29	0.23	0.42	0.43	0.40	0.66	0.79	0.64	0.58
Al ₂ O ₃	16.82	19.91	14.24	11.73	15.30	16.08	15.90	18.43	17.09	16.33	15.90
Fe ₂ O ₃	3.69	7.61	3.23	1.69	3.15	3.38	2.67	7.70	5.90	5.42	3.47
MnO	0.08	0.16	0.02	0.03	0.11	0.04	0.07	0.14	0.09	0.10	0.07
MgO	1.50	3.93	0.53	0.46	0.88	0.62	0.81	4.42	1.84	2.48	1.34
CaO	2.19	5.45	2.35	2.36	3.67	3.43	2.89	8.78	6.07	5.91	4.31
Na ₂ O	2.61	1.73	3.28	2.85	3.49	3.56	4.19	2.90	3.57	3.35	3.76
K ₂ O	7.24	6.11	3.36	2.31	2.98	2.63	3.61	1.41	2.71	1.91	2.69
P ₂ O ₅	0.05	0.08	0.04	0.05	0.11	0.09	0.11	0.09	0.20	0.09	0.10
BaO	0.35	0.34	0.06	0.05	0.06	0.06	0.10	0.03	0.13	0.04	0.04
L.O.I.	0.17	0.21	0.12	0.20	0.19	0.09	0.12	0.06	0.09	0.04	0.48
Total	100.03	100.00	100.57	98.53	99.92	99.98	99.45	100.34	100.39	100.08	100.77

471
472 The classification of rock type for each sample is on the basis of field observation and SiO₂ versus K₂O plot of Le Bas et al. (1986). All iron expressed as Fe₂O₃(total).

473



474

475

476

477

478

479

480

481

Figure 11. Eruption age versus (A) cumulative eruption volume for the volcanic deposits of Milos, (B) SiO₂ wt.%, (C) K₂O%/SiO₂%, of Milos volcanic units of this study and previous studies. The maximum (Max; red line) and minimum (Min; dashed red line) cumulative eruption volume curves were estimated from Campos et al. (1996) and Stewart and McPhie (2006). Q_e is the long-term volumetric volcanic output rate (see discussion). The exact volume of volcanic products between 4.1 and 3.08 Ma is not well constrained and indicated with a question mark. The major element data of the old pumices of Filakopi volcanoes (2.66 Ma) are from Stewart (2003). The major element data of the Plakes lava dome is from Fytikas et al. (1986). Geochemical data of the old pumices of the Profitis Illias (~3.08 Ma) is lacking due to the severe alteration.

482

4 Discussion

483

4.1 Comparison with the previous geochronological studies on the Milos VF

484

485

486

487

488

489

490

491

492

493

494

495

More than half of our ⁴⁰Ar/³⁹Ar ages derived for this study are based on high-resolution laser incremental heating method. All incremental step heating experiments are reproducible, except for the sample G15M0017 which gave the oldest age. The total fusion experiments of this study gave at least five times smaller analytical uncertainty (1SE on average ≤0.01 Ma) than the previous studies using conventional K-Ar (Angelier et al., 1977; Fytikas et al., 1976, 1986; Matsuda et al., 1999) and SHRIMP U/Pb zircon methods (Stewart and McPhie, 2006). Fission track dating on obsidians of the Milos VF produced two ages (Bigazzi and Radi, 1981; Arias et al., 2006) which seems to overlap with the K-Ar and ⁴⁰Ar/³⁹Ar ages, but with larger uncertainty. U/Pb zircon ages could indicate the timing of zircon formation at high temperature (>1000 °C) in magma chambers significantly prior to volcanic eruption (e.g. Flowers et al., 2005). On the other hand, the lower closure temperature of K-rich minerals (<700 °C) makes the K-Ar and ⁴⁰Ar/³⁹Ar ages better suited to determine the timing of extrusion of volcanic products (e.g. Grove and Harrison, 1996; Cassata and Renne, 2013).

The MSWD value, as a measure of the scatter of the individual step ages, is based on the error enveloping around the data point. The decrease in error will automatically cause an increase in MSWD (e.g. York, 1968; Wendt and Carl, 1991). The

496 MSWD values reported in this study are relatively high. In part this is caused by the fact that modern multi-collector mass
497 spectrometers used for $^{40}\text{Ar}/^{39}\text{Ar}$ dating can measure the isotope ratios very precisely, which in turn would increase the MSWD.
498 It will be more valuable and challenging to find a plateau or isochron age which meets the MSWD criteria (<2.5) by modern
499 multi-collector $^{40}\text{Ar}/^{39}\text{Ar}$ dating than by K-Ar or $^{40}\text{Ar}/^{39}\text{Ar}$ dating using a single detector instrument (e.g. Mark et al., 2009).
500 Potential drawbacks of the $^{40}\text{Ar}/^{39}\text{Ar}$ method are its dependence on neutron irradiation causing the production of interfering
501 argon isotopes that need to be corrected for. The uncertainty in the ages of standards that are required to quantify the neutron
502 flux also needs to be incorporated in the final ages as are uncertainties related to decay constants (supplementary material II).
503 Finally, recoil can occur during irradiation. Minerals such as biotite can be prone to recoil, yielding slightly older ages (e.g.
504 Hora et al., 2010).

505 In this section, our $^{40}\text{Ar}/^{39}\text{Ar}$ results are compared with previously published geochronological data, and subsequently used to
506 refine the stratigraphy of the Milos VF. In the last part, we will discuss the temporal variations in major elements and the
507 volumetric volcanic output rate of the Milos VF.

508 Figure 12 compares previous published K-Ar, U/Pb zircon and fission track ages from the same volcanic units with the new
509 $^{40}\text{Ar}/^{39}\text{Ar}$ data of this study. In general, there is a good agreement, however, six ages out of twenty-three differ significantly
510 from previous studies and will be discussed below.

511 The obsidian fission track ages (Bigazzi and Radi, 1981; Arias et al., 2006) for the Dhemenehaki volcano are 0.25 My younger
512 than the K-Ar ages (1.84 Ma, Angelier et al., 1977) and the $^{40}\text{Ar}/^{39}\text{Ar}$ age of this study (1.825 Ma, G15M0032B). The good
513 agreement between the K-Ar and $^{40}\text{Ar}/^{39}\text{Ar}$ ages suggests that the fission track ages record another, lower temperature event,
514 than the K-Ar and $^{40}\text{Ar}/^{39}\text{Ar}$ ages. In addition, the larger uncertainty of fission track ages (>0.05 Ma) also overlaps with the
515 $^{40}\text{Ar}/^{39}\text{Ar}$ age at 2-sigma. We assume that the $^{40}\text{Ar}/^{39}\text{Ar}$ age is the correct extrusion age for the obsidian of the Dhemenehaki
516 volcano.

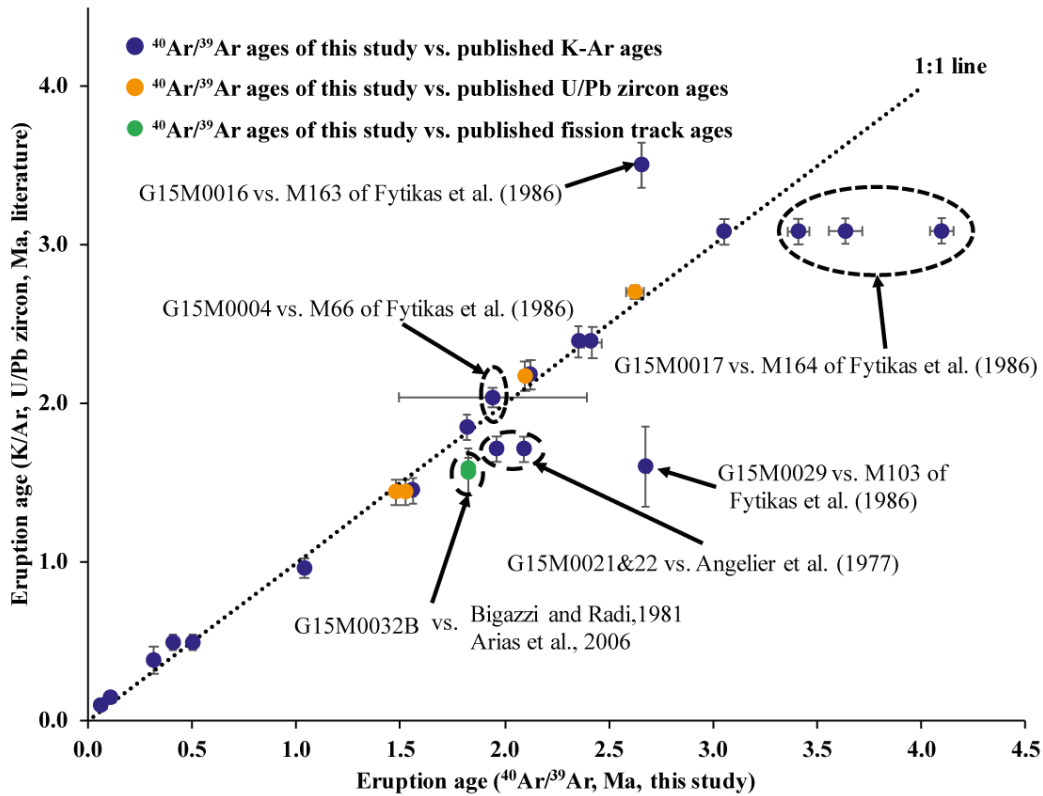
517 Angelier et al. (1977) reported one dacite sample in the northwest of Milos with an age of 1.71 Ma (Angelier_3, location 3 on
518 Figure 3 of Angelier et al., 1977). Argon loss could result in these ages (Angelier_3-5 in Figure 12) being younger than our
519 $^{40}\text{Ar}/^{39}\text{Ar}$ groundmass ages of 1.97 ± 0.01 Ma (dacite sample G15M0021 and -22).

520 The amphibole of sample G15M0004 of the Adamas dacitic lava dome, located ~ 1 km north of rhyolitic Bombarda volcano,
521 gave an inverse isochron age of $1.95 \text{ Ma} \pm 0.45 \text{ Ma}$. This age overlaps with the K-Ar age for the Adamas lava dome of $2.03 \pm$
522 0.06 Ma (dacite M 66) of Fytikas et al. (1986). The large analytical uncertainty of our sample G15M0004 is caused by a
523 combination of low $^{40}\text{Ar}^*$ yields and clustering of data points that define the inverse isochron showing excess argon was
524 identified by the $^{40}\text{Ar}/^{39}\text{Ar}$ method ($^{40}\text{Ar}/^{36}\text{Ar} 319.51 \pm 14.70$), whereas the presence of excess argon cannot be tested by the
525 K-Ar technique, implying that the Fytikas et al. (1986) might be slightly old.

526 The Korakia andesite has an age of $1.59 \pm 0.25 \text{ Ma}$ (M 103, Fytikas et al., 1986) and was deposited in a submarine-subaerial
527 environment on top of the Sarakiniko Formation that was dated based on paleomagnetic polarity in combination with a K-Ar
528 age (1.80-1.85 Ma, Stewart and McPhie, 2003 and reference therein). The much older $^{40}\text{Ar}/^{39}\text{Ar}$ groundmass age (2.68 ± 0.01
529 Ma) of Korakia andesite sample G15M0029 is unreliable and it could indicate the emplacement age of the Kalogeros
530 cryptodome ($2.70 \pm 0.04 \text{ Ma}$, Stewart and McPhie, 2006) or represents a geological meaningless age with only 23-27% of the
531 total ^{39}Ar released in the “plateau”. In this case, the K-Ar age of $1.59 \pm 0.25 \text{ Ma}$ is considered as the likely eruption age for the
532 Korakia andesite although its argon loss or excess Ar component is unknown.

533 We obtained $^{40}\text{Ar}/^{39}\text{Ar}$ ages of 3.41-4.10 Ma and $3.06 \pm 0.02 \text{ Ma}$, respectively, from the groundmasses of dacite samples
534 G15M0017 and G15M0015 in the southwest of Milos (Figure 2 and 13B). Both of these samples are derived from the coherent
535 dacite facies of the rhyolitic Profitis Ilias volcano based on the Figure 11 of Stewart and McPhie (2006). Sample G15M0015
536 yielded much higher radiogenic ^{40}Ar (41.77%) than that of sample G15M0017 ($<10\%$ of $^{40}\text{Ar}^*$), and the rhyolite sample M
537 164 from Fytikas et al. (1986) (23.5% of $^{40}\text{Ar}^*$) gave an estimate the eruptive age of $3.08 \pm 0.08 \text{ Ma}$ to the Profitis Ilias

538 volcano which is much younger than that given by our sample G15M0017 (Figure 12). Therefore, we consider our $^{40}\text{Ar}/^{39}\text{Ar}$
 539 ages of 3.06 ± 0.02 Ma as the best estimate of the emplacement age of the coherent dacite facies of Profitis Illias volcano.
 540 A basaltic andesite dyke near Kleftiko on the south-western coast of Milos has a K-Ar age of 3.50 ± 0.14 Ma which only gave
 541 13.9% of $^{40}\text{Ar}^*$ (Fytikas et al. 1986). This age is significantly older than the eruptive ages of Profitis Illias volcano which the
 542 dyke intruded (Stewart, 2003). Although containing relatively low $^{40}\text{Ar}^*$ (16.87%), our $^{40}\text{Ar}/^{39}\text{Ar}$ age of 2.66 ± 0.01 Ma with
 543 67.27% of $^{40}\text{Ar}^*$ from the groundmass of basaltic andesitic sample G15M0016 of the dyke near Kleftiko is probably an accurate
 544 intrusion age.



545
 546 **Figure 12.** The $^{40}\text{Ar}/^{39}\text{Ar}$ ages of this study (x-axis) compared to the K/Ar ages (Angelier et al., 1977; Fytikas et al., 1986), U/Pb
 547 zircon ages (Stewart and McPhie, 2006) and fission track ages (Bigazzi and Radi, 1981; Arias et al., 2006) (y-axis) for the same
 548 volcanic units. Ages which deviate from the 1:1 correlation line are discussed in section 4.1.

549 **4.2 The published ages of other volcanic units**

550 Unfortunately, we were not able to date all key volcanic units of the Milos VF. This was due to three reasons: (1) we did not
 551 collect samples from all units; (2) some of the collected samples were not fresh enough after inspection of thin sections; and
 552 (3) some of the $^{40}\text{Ar}/^{39}\text{Ar}$ data indicate that the K-Ar decay system was disturbed. Therefore, we include published age
 553 information to establish a complete high-resolution geochronology for the Milos VF.

554 The published volcanic units that we include are the Profitis Illias volcano (3.08 ± 0.08 Ma with 23.5 (%), Fytikas et al., 1986),
 555 the Mavro Vouni lava dome (2.50 ± 0.09 Ma with 55.2 $^{40}\text{Ar}^*$ (%), Anglier et al., 1977) in the south-western part of Milos, the
 556 Bombarda volcano (1.71 ± 0.05 Ma with 24.3 $^{40}\text{Ar}^*$ (%), Fytikas et al., 1986), the Plakes volcano (0.97 ± 0.06 Ma with 10.2
 557 $^{40}\text{Ar}^*$ (%), Fytikas et al., 1986, and 0.8-1.2 Ma with 5.4-11.9 $^{40}\text{Ar}^*$ (%) Matsuda et al. 1999). Scoria deposits that Stewart and
 558 McPhie (2006) attributed to an andesitic scoria cone between Milos and Kimolos were produced in submarine, and maybe
 559 occasionally above sea level. No age data for this deposit has been published so far. However, the stratigraphic position of this
 560 scoria deposit is between MIL 365 (2.66 Ma, Stewart and McPhie, 2006) and M103 (1.59 Ma, Fytikas et al., 1986), which is
 561 shown in Figure 10 of Stewart and McPhie (2006). Therefore, this scoria cone was likely active in the north-eastern part of the
 562 Milos VF between 2.6 and 1.6 Ma.

563 Fytikas et al. (1986) also analysed a pumice coming from the Sarakiniko deposits east of Adamas (1.85 ± 0.10 Ma with 13.6
 564 $^{40}\text{Ar}^*$ (%), Fytikas et al., 1986) (Fig. 2). This unit is reworked pyroclastic sediment of the Adamas lava dome (Rinaldi and

565 Venuti, 2003). Therefore, the K-Ar age from the Sarakiniko unit is not considered as an eruption age in this study. We did not
566 sample the neighbouring islands of the Milos VF and also did not attempt to date the products of the recent phase of phreatic
567 activity from which Traineau and Dalabakis (1989) obtained ^{14}C ages of 200 BC and 200 AD.

568 **4.3 Implications for the stratigraphy of the Milos VF**

569 **4.3.1. Start of volcanism in the Milos VF**

570 Figures 13 and 14 summarize our new $^{40}\text{Ar}/^{39}\text{Ar}$ ages in combination with previously published stratigraphic, biostratigraphic,
571 fission track, ^{14}C , K-Ar and U-Pb age data. We did not consider the Matsuda et al. (1999) data as the fission-track ages seem
572 to be offset to other dating techniques ages obtained from the same deposits (see section 4.1 above). The exact start of
573 volcanism in the Milos VF is still unclear since these older deposits are strongly hydrothermally altered. Van Hinsbergen et al.
574 (2004) reported five ash layers in the Pliocene sedimentary rocks of southern Milos, ranging between 4.5-3.7 Ma in age, based
575 on biostratigraphy, magnetostratigraphy and astronomical dating. In a slightly wider circle around Milos island, the $6.943 \pm$
576 0.005 Ma a1-tephra event recorded in several locations on nearby Crete (Rivera et al., 2011) shows that explosive volcanism
577 along the Aegean arc, possibly on Milos, already occurred during the Messinian. These ash beds cannot be traced to currently
578 exposed centres in the Milos VF and could conceivably be related to volcanic centres further north (Antiparos and Patmos),
579 which were active during this time interval (Vougioukalakis et al., 2019).

580 Biostratigraphy shows that the youngest layer with dateable fossils (bio-event, the last common occurrence of *Sphenolithus*
581 spp., Van Hinsbergen et al., 2004) in the Neogene sedimentary rocks is 3.61 Ma old (GTS2020, Raffi et al., 2020). The
582 diatomite Unit II from Calvo et al. (2012) on top of the oldest volcanoclastic deposit from the north-eastern coast of Milos is
583 constrained within 2.83-3.19 Ma. These data suggest that the oldest products must be older than 2.83 Ma and younger than
584 3.61 Ma. Our oldest $^{40}\text{Ar}/^{39}\text{Ar}$ ages of this study displayed a wide range of 3.41-4.10 Ma that is probably not correct due to
585 alteration of the samples. Alteration might induce Ar loss and that would imply that the age is even older than 3.4-4.1 Ma. The
586 age of 3.50 ± 0.14 Ma given by Fytikas et al. (1986) for an andesitic pillow lava or dyke has been discussed above and probably
587 belongs to a series of basaltic andesite intrusions in the younger dacitic-rhyolitic deposits of Profitis Ilias (~ 3.08 Ma, Fytikas
588 et al., 1986), and therefore the 3.5 Ma age is probably not correct (e.g. Stewart, 2003). Fytikas et al. (1986) measured one
589 sample from Kimolos (Figure 2 and 3) with an age of 3.34 Ma. Furthermore, Ferrara et al. (1980) reported an age of 3.15 Ma
590 for a lithic clast derived from the Petalia intrusion in the Kastro volcanoclastics of Polyegos. If we assume that this reported
591 age is a cooling age, volcanism in the Milos VF must have started before 3.15 Ma. Although age constraints for the start of
592 volcanism on Milos both from the Neogene sedimentary rocks and the dated volcanic samples are poor, the evidence at this
593 stage would suggest that volcanism in the Milos VF started ~ 3.3 Ma ago.

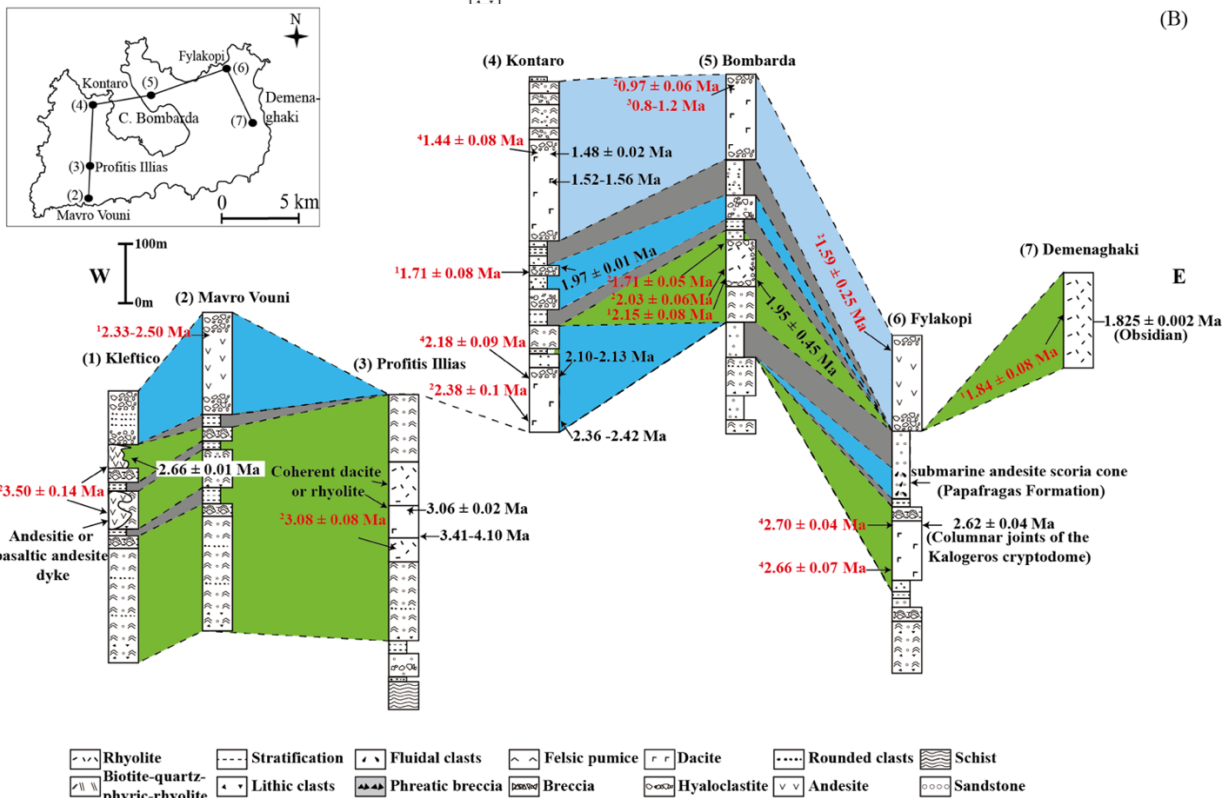
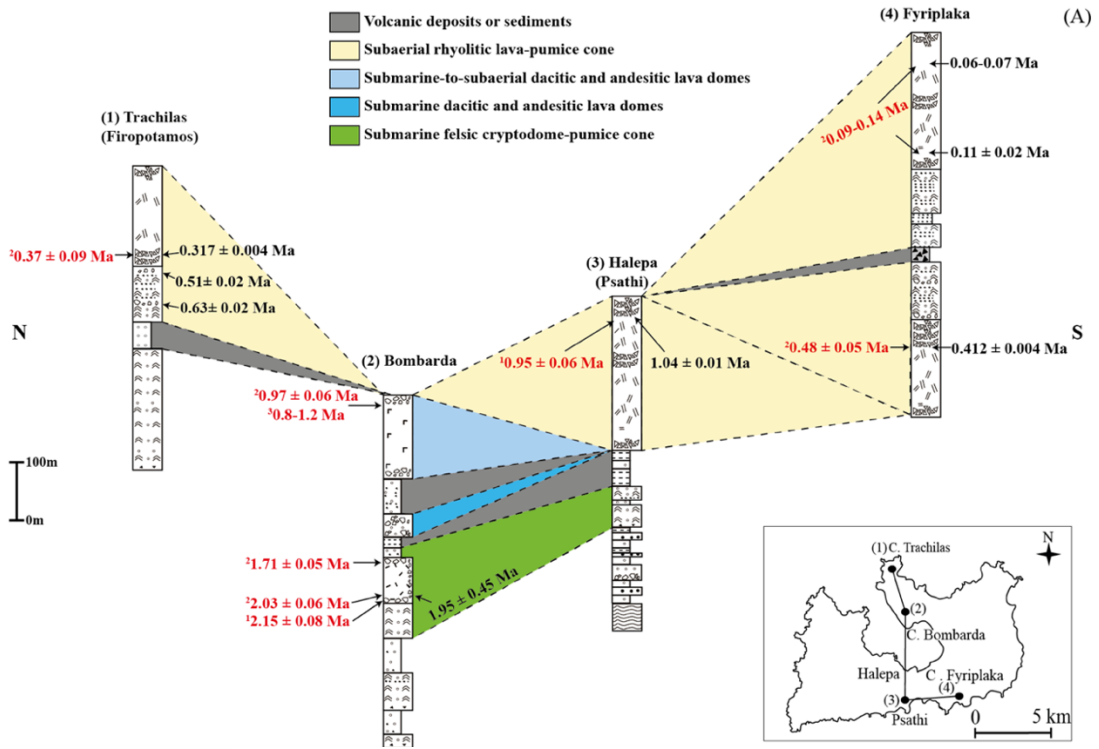


Figure 13. Nine selected stratigraphic columns covering the (A) young (<1.4 Ma) and (B) old (>1.4 Ma) volcanic deposits of Milos modified after Stewart and McPhie (2006), except for (7) Demenaghaki. Age data in black are from this study and in red are from: 1=Angelier et al. (1977), 2=Fytikas et al. (1976, 1986), 3=Matsuda et al. (1999), 4=Stewart and McPhie (2006).

4.3.2. Periods with different volumetric output

The volume estimates of the Milos VF are hampered by limited exposure of several volcanic units and unknown age relationships. Therefore, not all units can be attributed to a certain volcano. Furthermore, we also do not know how much the volcanic products were lost through transport by air, sea currents and erosion. Therefore, the discussion here only provides a first order estimate of the onshore extruded magma volume. Taken into account all these limitations, our age data and the volume estimates by Stewart and McPhie (2006) indicate at least three periods of different long-term volumetric volcanic

605 output rates (Q_e) from ~ 3.3 to 0.0 Ma. We define a “Period” as a time interval where the Q_e is significantly different from the
606 average output rate (Q_e average = $1.0 \times 10^{-5} \text{ km}^3 \cdot \text{yr}^{-1}$) of the Milos VF over the last 3.3 Ma. Figure 11 shows that the Q_e can be
607 subdivided into two slow-growth periods (I and III) and one period (II) during which the Q_e was significantly larger.
608 The lower boundary of Period I is based on our estimate of the oldest volcanic units of Milos at ~ 3.3 Ma. These oldest units
609 were deposited in the southwest of Milos between ~ 3.3 and 3.08 Ma and include the BPS of Fytikas et al. (1986) and the felsic
610 pumice cone/crypto dome facies of Stewart and McPhie (2006). These deposits have a minimum thickness of 120 m. The
611 estimates of the DRE volume and Q_e of these earliest volcanic deposits are hampered by the lack of precise age information,
612 the high degree of alteration and structural complexities. Therefore, we only calculated the Q_e of Period I from 3.08 Ma for
613 which the eruption products are mainly dacitic-rhyolitic in composition (Table 5, Fig 11), and the first products that can be
614 reliably dated are cryptodomes (3.06 Ma, sample G15M0015) and dykes (2.66 Ma, sample G15M0016) into the BPS of Fytikas
615 et al. (1986) or the units of Profitis Illias volcano of Stewart and McPhie (2006, 3.08 Ma) in the southwest of Milos. These
616 cryptodomes and dykes were followed by the formation of the submarine Fylakopi pumice cone volcano at 2.66 Ma (Stewart
617 and McPhie, 2006) and Kalogeros cryptodome at 2.62 Ma (sample G15M0006) in the north-eastern part of Milos. These two
618 pumice cone volcanoes contributed 3-11 km^3 DRE in volume to the Milos VF. The last two volcanic activities of Period I
619 occurred in the southwest (Mavro Vauni, 2.50 Ma, Angelier et al., 1977) and west of Milos (Mavros Kavos, 2.36 Ma, this
620 study), respectively, which produced two high-aspect-ratio andesitic-dacitic lava domes with a total volume of 1-3 km^3 DRE
621 (Stewart and McPhie, 2006). During the submarine Period I, which lasted ~ 1.2 Ma, the estimated Q_e is $0.9 \pm 0.5 \times 10^{-5} \text{ km}^3 \cdot \text{yr}^{-1}$.
622

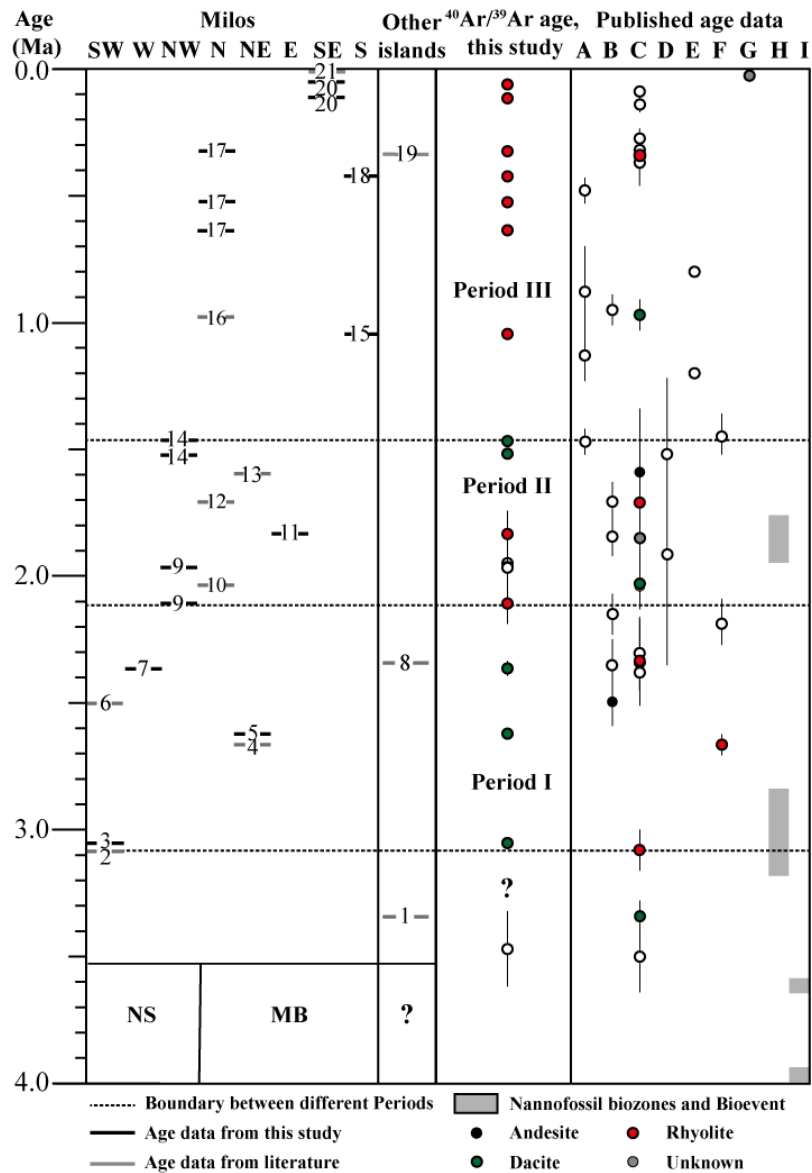
Table 5. Summary of the eruption ages of the Milos volcanic field

No.	Name of volcanic centre	Age (Ma)	Reference
1	Kimlos volcano	3.34	Fytikas et al., 1986
2	Profitis Illias crypto/pumice cone	3.08	Fytikas et al., 1986
3	coherent dacite of Profitis Illias volcano	3.06	This study
4	Filakopi volcano	2.66	Stewart and McPhie, 2006
5	Kalegeros cryptodome	2.62	This study
6	Mavro Vouni lava dome	2.5	Angelier et al., 1977
7	Mavros Kavos lava dome	2.42-2.36	This study
8	Polyegos lava dome	2.34	Fytikas et al., 1986
9	Triades lava dome	2.13-2.10 and 1.97	This study
10	Adamas lava dome	2.03	Fytikas et al., 1986
11	Dhemeneghaki volcano	1.83	This study
12	Bombardo volcano	1.71	Fytikas et al., 1986
13	Korakia dome	1.59	Fytikas et al., 1986
14	Komntaro dome	1.52-1.48	This study
15	Halepa lava dome	1.04	This study
16	Plakes lava dome	0.97	Fytikas et al., 1986
17	Trachilias complex	0.63, 0.51 and 0.317	This study
18	Kalamos lava dome	0.41	This study
19	Antimilos domes	0.32	Fytikas et al., 1986
20	Fyriplaka complex	0.11 and 0.07-0.06	This study
21	Phreatic activity	200 AD-200 BC	Trainau and Dalabakis, 1989

623
624 The change from Period I to II is based on the sharp increase in Q_e at 2.13 Ma (Fig. 11). During this period the Q_e ($3.0 \pm$
625 $1.7 \times 10^{-5} \text{ km}^3 \cdot \text{yr}^{-1}$) increased by a factor of ~ 3 compared to Period I and III. Period II began with the submarine extrusions of
626 the dacitic-rhyolitic Triades lava dome in the north-west and dacitic Adamas lava dome in the north-east of Milos and was
627 followed by the rhyolitic Dhemeneghaki pumice cone/cryptodome and the Bombardo volcano in the north-east of Milos. For
628 the Bombarda centre a large age range is reported in the literature (1.71-2.15 Ma, Fig. 13B). We did not successfully date
629 samples from the Bombarda centre, but Rinaldi and Campos Venuti (2003) reported that an age of 1.71 Ma is the best
630 approximation based on other stratigraphic information. For the Dhemeneghaki centre, we obtained a $^{40}\text{Ar}/^{39}\text{Ar}$ age of 1.825
631 ± 0.002 Ma from obsidian. The Triades, Adamas, Dhemeneghaki and Bombarda centres all developed in submarine settings,
632 as the intercalated sediments from the northern coast of Milos show (Calvo et al., 2012; Fig. 14). The last two volcanic

633 expressions in Period II consist of two submarine-to-subaerial lava dome extrusions, Kantaro (1.59 Ma, Fytikas et al., 1987)
634 and Korakia (1.48 Ma, this study) in the north-west and north-east of Milos, respectively. The products of these two centres
635 are andesitic-dacitic in composition. All volcanic centres of Period II produced 8-30 km³ DRE in volume for the Milos VF.
636 Period III began with a time interval of 0.4 Ma with no eruptions and has a very low Q_e of $0.25 \pm 0.05 \times 10^{-5} \text{ km}^3 \cdot \text{yr}^{-1}$. The
637 boundary between Period II and III can be placed at the last eruption of Period II, at the start of the first eruption in the low
638 output interval, or halfway in between. The difference between those options is not significant, given the large uncertainties
639 of the volume estimates (Fig. 12), and therefore we have decided to start Period III directly after the last eruption of the high
640 Q_e of Period II. The composition of nearly all Period III volcanic products is rhyolitic, an exception is the dacitic Plakes lava
641 dome (Fig. 12). The Plakes lava dome is probably the last volcano erupting at ~ 0.97 Ma (Fytikas et al., 1987) in a submarine
642 environment in the north of Milos, whereas the other lava dome in Period III, Halepa, produced rhyolitic lavas in a subaerial
643 setting in the south (Stewart and McPhie, 2006). The Halepa and Plakes domes contributed 1-3 km³ DRE in volume to the
644 Milos VF and were followed by a 0.3 Ma interval with no or limited volcanic eruptions. Two subaerial pumice cone volcanoes
645 with biotite bearing rhyolites were constructed during the last 0.6 Ma, the Trachilias and Fyriplaka complexes. The Trachilias
646 complex was active for approximately 300 kyr (0.63-0.32 Ma) in the northern part of Milos. The evolution of this complex
647 began with phreatic eruptions which became less explosive over time (Fytikas et al., 1986). During the last eruption ($0.317 \pm$
648 0.004 Ma) of the Trachilias complex rhyolitic pumices filled up the crater area and did breach the northern tuff cone walls. The
649 Trachilias complex only added a small volume (1-2 km³ DRE) to the Milos VF. The Kalamos lava dome was also extruded in
650 the south of Milos (Fig. 2) contemporaneously with the Trachilias complex.

651 The youngest volcanic activity of Milos (0.11 Ma-present) is characterized by subaerial eruptions of biotite phyric rhyolite
652 from the Fyriplaka complex in the south of Milos, and was studied in detail by Campos Venuti and Rossi (1996). This complex
653 is constructed on a paleosol that developed in a phreatic deposit (“Green Lahar”, Fytikas et al., 1986) or lies directly on the
654 metamorphic basement. Campos Venuti and Rossi (1996) indicated that the stratigraphic order is: Fyriplaka and Gheraki tuff
655 rings, Fyriplaka lava flow, tuff cone of Tsigrado-Provatas. The total estimated volume of volcanic material is 0.18 km³ DRE.
656 The boundary between the Fyriplaka and Tsigrado tuff cones is characterized by a marked erosive unconformity. The
657 composition of these young volcanic products is very constant (Fig. 10-11), as noted by Fytikas et al. (1986) and Campos
658 Venuti and Rossi (1996). The products from Fyriplaka and Tsigrado cones are covered by a paleosol rich in archaeological
659 remains and a phreatic deposit consisting largely of greenschist metamorphic fragments. According to Campos Venuti and
660 Rossi (1996), the Fyriplaka cone was quickly built by phreatic and phreatomagmatic eruptions, as there are no paleosols
661 observed between the different units. However, our data do suggest a large range in ages between 0.11 and 0.06 Ma. Fytikas
662 et al. (1986) also reported a range between 0.14 and 0.09 Ma. These ages are inconsistent with the “Green Lahar” age of 27
663 kyrs (Principe et al., 2002), suggesting that the “Green Lahar” deposit consists of many different phreatic eruption layers that
664 were formed during a time interval of more than 0.4 Ma, as the Kalamos lava is underlain by a green phreatic eruption breccia
665 (Campos Venuti and Rossi 1996). We, therefore, conclude that phreatic eruptions occurred for more than 400 kyr,
666 predominantly in the eastern part of Milos until historical times (200 BC – 200 AD, Traineau and Dalabakis, 1989).



667
668
669
670
671
672
673
674
675
676
677
678
679

Figure 14. Diagram presenting three periods of different long-term volumetric volcanic output rate on Milos volcanic field based on the new $^{40}\text{Ar}/^{39}\text{Ar}$ data of this study and published data. The location of the different volcanoes is given in Fig 2 and indicated in the left panel (from left to right: SW, W, NW, N, NE, E, SE and S of Milos). The right panel corresponds to published age data: [A]=Fytikas et al., 1976, [B]=Angelier et al., 1977, [C]=Fytikas et al., 1986, [D]= Bigazzi & Radi, 1981, [E]=Matsuda, 1999, [F]=Stewart and McPhie (2006), [G]= Trainau and Dalabakis, 1989, and Biostratigraphic data of the Neogene sediments (NG) is from [H]=Calvo et al. (2012) and [I]=Van Hinsbergen et al. (2004) calibrated to Raffi et al. (2020) (LCO of *Sphenolithus* spp. and FO of *D. tamalis*). The number in the left panel represents the volcanic centres of Milos (see details in Table 5). The start of volcanism (3.08-3.61 Ma) on Milos and the basement of the other Islands (Antimilos, Kimolos and Polyegos) are not well constrained and indicated with question marks (see text for discussion). The simplified basement cross-section (NS: Neogene sedimentary rock; MB: Metamorphic basement) under Milos volcanic units is based on Fytikas et al. (1989). We used the filled symbols as the best estimate for the eruption ages at the different volcanic centres, and the open symbols are not used as the best estimate due to their relatively large uncertainties.

680 4.3.3 Temporal evolution of the magma flux and composition

681 Figure 11 shows temporal major-element variations during the evolution of the Milos VF. The volcanic units of Period III are
682 dominantly rhyolitic in composition, whereas during Period I and II the compositions of volcanic units range between basaltic-
683 andesite to rhyolite. However, the $\text{K}_2\text{O}/\text{SiO}_2$ ratio is constant (0.05 ± 0.02) over the 3.3 Ma evolution of the Milos VF, with
684 one exception, sample G15M0021 collected near Cape Vani which is altered by hydrothermal processes (e.g. Alfieris et al.
685 2013). Period I and III contain large explosive pumice cone volcanoes, whereas Period II is dominated by effusive dome
686 extrusions. The difference in volcanic structures is not observed in the SiO_2 content and the $\text{K}_2\text{O}/\text{SiO}_2$ ratio of the volcanic
687 products.

688 It is noteworthy that the value of the Q_e ($0.2-4.7 \times 10^{-5} \text{ km}^3 \cdot \text{yr}^{-1}$) for the Milos VF is at least 2-3 orders lower than the average
689 for rhyolitic systems ($4.0 \times 10^{-3} \text{ km}^3 \cdot \text{yr}^{-1}$) and the mean for continental arcs ($\sim 70 \times 10^{-3} \text{ km}^3 \cdot \text{yr}^{-1}$) (White et al., 2006). Milos
690 overlaps with the lowest Q_e values of the study of White et al. (2006). No data are available for the ratio between intruded
691 magma in the crust below Milos and extruded volcanic units (I:E). White et al. (2006) argued that a ratio of 5:1 (I:E) is probably
692 a realistic estimate for most volcanic centres and that this ratio can be higher in volcanic centres constructed on continental
693 crust. A magma supply rate from the mantle beneath the Milos VF could be estimated in the order of $0.1-3.3 \times 10^{-4} \text{ km}^3 \cdot \text{yr}^{-1}$.
694 Druitt et al. (2019) reported a long-term average magma supply rate of approximately $1 \times 10^{-3} \text{ km}^3 \cdot \text{yr}^{-1}$ beneath the Kameni
695 islands of Santorini, which is comparable to that of the Milos. Besides the case of Santorini VF, no other information on the
696 long-term average magma supply rate of other volcanic centres of the SAVA is available to our knowledge.
697 Milos is approximately 15 km long (W-E), a magma production rate of approximately $0.7-22 \text{ km}^3 \cdot \text{km}^{-1} \cdot \text{Ma}^{-1}$ can be estimated
698 over the last ~ 3.34 Ma. Although this magma production rate per km arc length is the onshore estimate for the Milos VF, it is
699 still significantly lower than for oceanic arcs: $157-220 \text{ km}^3 \cdot \text{Ma}^{-1} \cdot \text{km}^{-1}$ (Jicha and Jagoutz, 2015). For continental arcs, the long-
700 term magma production rate is more difficult to establish because magmatism is cyclic, and short periods (5-20 Ma) of intense
701 magmatism (“flare ups”) with $85 \text{ km}^3 \cdot \text{km}^{-1} \cdot \text{Ma}^{-1}$ being alternated with periods of 25-50 Ma of low magma production rate of
702 $20 \text{ km}^3 \cdot \text{km}^{-1} \cdot \text{Ma}^{-1}$ (e.g. Jicha and Jagoutz, 2015). The periods of low magma production overlap with the magma production
703 rates beneath the Milos VF over the past ~ 3.34 Ma.

704 5 Conclusions

705 This study reports twenty-one new $^{40}\text{Ar}/^{39}\text{Ar}$ ages and major element data for 10 volcanic units of the Milos Volcanic Field.
706 In combination with previously published age data, geochemistry and facies analysis the following points can be made.

- 707 (1) The exact age of the start of volcanism in the Milos VF is still unclear due to the high degree of alteration of the oldest
708 deposits. The best estimate based on our new $^{40}\text{Ar}/^{39}\text{Ar}$ ages, published K-Ar data and nannofossil biozones is between
709 3.5 and 3.15 Ma.
- 710 (2) Based on the long-term volumetric volcanic output rate, the volcanic history of the Milos VF can be divided into two
711 slow growth periods, Period I ($\sim 3.3-2.13$ Ma) and III (1.48 Ma-present), and one relatively fast growth period, Period
712 II (2.13-1.48 Ma).
- 713 (3) Period I and II are characterised by andesitic to rhyolitic lavas and pyroclastic units, whereas those of Period III are
714 dominantly rhyolitic. The $\text{K}_2\text{O}/\text{SiO}_2$ ratio is constant over the 3.3 Ma history of the Milos VF.
- 715 (4) The long-term volumetric volcanic output rate of Milos is $0.2-4.7 \times 10^{-5} \text{ km}^3 \cdot \text{yr}^{-1}$, two-three orders of magnitude lower
716 than the average for rhyolitic systems and continental arcs.

717 Acknowledgement

718 We would like to thank Roel van Elsas for the assistance with rock crushing and mineral separation. Kiki Dings helped with
719 the XRF bead preparation and measurements. Lara Borst and Onno Postma assisted with the $^{40}\text{Ar}/^{39}\text{Ar}$ dating. We acknowledge
720 the Greek Institute of Geology and Mineral Exploration (IGME) for permission to conduct fieldwork on Milos. Xiaolong Zhou
721 would like to acknowledge a grant no. 201506400055 from the China Scholarship Council (CSC). The $^{40}\text{Ar}/^{39}\text{Ar}$ facility of the
722 VU is covered by NWO grant 834.09.004. This research benefitted from funding from the European Research Council under
723 the European Union's Seventh Framework Programme (FP7/2007-2013)/ERC grant agreement n° 319209. A previous version
724 of this manuscript greatly benefitted from a very detailed and constructive review by Dr. J. McPhie. A second review by Dr J.
725 McPhie, Dr. J-F. Wotzlav and Dr. Peter Abbott helped to clarify the interpretation of the geochronology of Milos. We thank
726 Drs. J. Nadden, J. Miles and S Tapster for pointing out mistakes in our figures.

- 728 Alfieris, D., Voudouris, P. and Spry, P. G.: Shallow submarine epithermal Pb-Zn-Cu-Au-Ag-Te mineralization on western
729 Milos Island, Aegean Volcanic Arc, Greece: Mineralogical, geological and geochemical constraints, *Ore Geol. Rev.*, 53,
730 159–180, doi:10.1016/j.oregeorev.2013.01.007, 2013.
- 731 Angelier, J., Cantagrel, J.-M. and Vilminot, J.-C.: Neotectonique cassante et volcanisme plio-quadernaire dans l'arc egeen
732 interne; l'île de Milos (Grece), *Bull. la Société Géologique Fr.*, 7(1), 119–124, 1977.
- 733 Arias, A., Oddone, M., Bigazzi, G., Di Muro, A., Principe, C. and Norelli, P.: New data for the characterization of Milos
734 obsidians, *J. Radioanal. Nucl. Chem.*, 268(2), 371–386, doi:10.1007/s10967-006-0183-9, 2006.
- 735 Berger, G. W. and York, D.: Geothermometry from $^{40}\text{Ar}/^{39}\text{Ar}$ dating experiments, *Geochim. Cosmochim. Acta*, 45(6), 795–
736 811, doi:10.1016/0016-7037(81)90109-5, 1981.
- 737 Bigazzi, G. and Radi, G.: Datazione con le tracce di fissione per l'identificazione della provenienza dei manufatti di
738 ossidiana, *Riv. di Sci. Preist.*, 36/1–2, 223–250, 1981.
- 739 Calvo, J. P., Triantaphyllou, M. V., Regueiro, M. and Stamatakis, M. G.: Alternating diatomaceous and volcanoclastic
740 deposits in Milos Island, Greece. A contribution to the upper Pliocene-lower Pleistocene stratigraphy of the Aegean Sea,
741 *Palaeogeogr. Palaeoclimatol. Palaeoecol.*, 321–322, 24–40, doi:10.1016/j.palaeo.2012.01.013, 2012.
- 742 Campos Venuti, M. and Rossi, P. L.: Depositional facies in the Fyriplaka rhyolitic tuff ring, Milos Island (Cyclades, Greece),
743 *Acta Vulcanol.*, 8, 173–192, 1996.
- 744 Cassata, W. S. and Renne, P. R.: Systematic variations of argon diffusion in feldspars and implications for
745 thermochronometry, *Geochim. Cosmochim. Acta*, 112, 251–287, doi:10.1016/j.gca.2013.02.030, 2013.
- 746 Cole, P. D., Calder, E. S., Sparks, R. S. J., Clarke, A. B., Druitt, T. H., Young, S. R., Herd, R. A., Harford, C. L. and Norton,
747 G. E.: Deposits from dome-collapse and fountain-collapse pyroclastic flows at Soufrière Hills Volcano, Montserrat, *Geol.*
748 *Soc. London, Mem.*, 21(1), 231–262, 2002.
- 749 Crosweller, H. S., Arora, B., Brown, S. K., Cottrell, E., Deligne, N. I., Guerrero, N. O., Hobbs, L., Kiyosugi, K., Loughlin,
750 S. C. and Lowndes, J.: Global database on large magnitude explosive volcanic eruptions (LaMEVE), *J. Appl. Volcanol.*,
751 1(1), 4, 2012.
- 752 Druitt, T. H., Edwards, L., Mellors, R. M., Pyle, D. M., Sparks, R. S. J., Lanphere, M., Davies, M. and Barreirio, B.:
753 Santorini Volcano, *Geol. Soc. Mem.*, 19 [online] Available from: <http://pubs.er.usgs.gov/publication/70094778>, 1999.
- 754 Druitt, T. H., Pyle, D. M. and Mather, T. A.: Santorini Volcano and its Plumbing System, *Elements*, 15(3), 177–184,
755 doi:10.2138/gselements.15.3.177, 2019.
- 756 Duermeijer, C. E., Nyst, M., Meijer, P. T., Langereis, C. G. and Spakman, W.: Neogene evolution of the Aegean arc:
757 Paleomagnetic and geodetic evidence for a rapid and young rotation phase, *Earth Planet. Sci. Lett.*, 176(3–4), 509–525,
758 doi:10.1016/S0012-821X(00)00023-6, 2000.
- 759 Ferrara, G., Fytikas, M., Giuliani, O. and Marinelli, G.: Age of the formation of the Aegean active volcanic arc, *Thera*
760 *Aegean world II*, 2, 37–41, 1980.
- 761 Flowers, R. M., Bowring, S. A., Tulloch, A. J. and Klepeis, K. A.: Tempo of burial and exhumation within the deep roots of
762 a magmatic arc, Fiordland, New Zealand, *Geology*, 33(1), 17–20, doi:10.1130/G21010.1, 2005.
- 763 Francalanci, L. and Zellmer, G. F.: Magma Genesis at the South Aegean Volcanic Arc, *Elements*, 15(3), 165–170,
764 doi:10.2138/gselements.15.3.165, 2019.
- 765 Francalanci, L., Vougioukalakis, G. E., Fytikas, M., Beccaluva, L., Bianchini, G. and Wilson, M.: Petrology and
766 volcanology of Kimolos and Polyegos volcanoes within the context of the South Aegean arc, Greece, *Spec. Pap. Soc. Am.*,
767 418, 33, 2007.
- 768 Frey, H. M., Lange, R. A., Hall, C. M. and Delgado-Granados, H.: Magma eruption rates constrained by $^{40}\text{Ar}/^{39}\text{Ar}$
769 chronology and GIS for the Ceboruco-San Pedro volcanic field, western Mexico, *Bull. Geol. Soc. Am.*, 116(3–4), 259–276,

770 doi:10.1130/B25321.1, 2004.

771 Fytikas, M., Giuliani, O., Innocenti, F., Marinelli, G. and Mazzuoli, R.: Geochronological data on recent magmatism of the
772 Aegean Sea, *Tectonophysics*, 31(1–2), T29–T34, doi:10.1016/0040-1951(76)90161-X, 1976.

773 Fytikas, M., 1977. *Geology and Geothermics of Milos Island*. Thesis, Thessaloniki University, 228 pp. (in Greek with
774 English summary).

775 Fytikas, M., Innocenti, F., Kolios, N., Manetti, P., Mazzuoli, R., Poli, G., Rita, F. and Villari, L.: Volcanology and petrology
776 of volcanic products from the island of Milos and neighbouring islets, *J. Volcanol. Geotherm. Res.*, 28(3–4), 297–317,
777 doi:10.1016/0377-0273(86)90028-4, 1986.

778 Fytikas, M.: Updating of the geological and geothermal research on Milos island, *Geothermics*, 18(4), 485–496,
779 doi:10.1016/0375-6505(89)90051-5, 1989.

780 Grasemann, B., Huet, B., Schneider, D. A., Rice, A. H. N., Lemonnier, N. and Tschegg, C.: Miocene postorogenic extension
781 of the Eocene synorogenic imbricated Hellenic subduction channel: New constraints from Milos (Cyclades, Greece), *Bull.*
782 *Geol. Soc. Am.*, 130(1–2), 238–262, doi:10.1130/B31731.1, 2018.

783 Grove, M. and Harrison, T. M.: $^{40}\text{Ar}^*$ diffusion in Fe-rich biotite, *Am. Mineral.*, 81(7–8), 940–951, 1996.

784 Hayes, G. P., Moore, G. L., Portner, D. E., Hearne, M., Flamme, H., Furtney, M. and Smoczyk, G. M.: Slab2, a
785 comprehensive subduction zone geometry model, *Science* (80-), 362(6410), 58–61, doi:10.1126/science.aat4723, 2018.

786 Hildreth, W. and Lanphere, M. A.: Potassium-argon geochronology of a basalt-andesite-dacite arc system: The Mount
787 Adams volcanic field, Cascade Range of southern Washington, *Geol. Soc. Am. Bull.*, 106(11), 1413–1429, 1994.

788 Hildreth, W., Fierstein, J. and Lanphere, M.: Eruptive history and geochronology of the Mount Baker volcanic field,
789 Washington, *Geol. Soc. Am. Bull.*, 115(6), 729–764, 2003a.

790 Hildreth, W., Lanphere, M. A. and Fierstein, J.: Geochronology and eruptive history of the Katmai volcanic cluster, Alaska
791 Peninsula, *Earth Planet. Sci. Lett.*, 214(1–2), 93–114, doi:10.1016/S0012-821X(03)00321-2, 2003b.

792 Van Hinsbergen, D. J. J., Snel, E., Garstman, S. A., Marunțeanu, M., Langereis, C. G., Wortel, M. J. R. and Meulenkamp, J.
793 E.: Vertical motions in the Aegean volcanic arc: Evidence for rapid subsidence preceding volcanic activity on Milos and
794 Aegina, *Mar. Geol.*, 209(1–4), 329–345, doi:10.1016/j.margeo.2004.06.006, 2004.

795 Hora, J. M., Singer, B. S., Jicha, B. R., Beard, B. L., Johnson, C. M., de Silva, S. and Salisbury, M.: Volcanic biotite-
796 sanidine $^{40}\text{Ar}/^{39}\text{Ar}$ age discordances reflect Ar partitioning and pre-eruption closure in biotite, *Geology*, 38(10), 923–926,
797 doi:10.1130/G31064.1, 2010.

798 IJlst, L.: A laboratory overflow-centrifuge for heavy liquid mineral separation, *Am. Mineral.*, 58, 1088–1093, 1973.

799 Jicha, B. R. and Jagoutz, O.: Magma production rates for intraoceanic arcs, *Elements*, 11(2), 105–112,
800 doi:10.2113/gselements.11.2.105, 2015.

801 Kiliass, S. P., Naden, J., Cheliotis, I., Shepherd, T. J., Constandinidou, H., Crossing, J. and Simos, I.: Epithermal gold
802 mineralisation in the active Aegen volcanic arc: The Profitis Ilias deposits, Milos Island, Greece, *Miner. Depos.*, 36(1), 32–
803 44, doi:10.1007/s001260050284, 2001.

804 Koppers, A. A. P.: ArArCALC-software for $^{40}\text{Ar}/^{39}\text{Ar}$ age calculations, *Comput. Geosci.*, 28(5), 605–619,
805 doi:10.1016/S0098-3004(01)00095-4, 2002.

806 Kornprobst, J., Kienast, J.-R. and Vilminot, J.-C.: The high-pressure assemblages at Milos, Greece, *Contrib. to Mineral.*
807 *Petrol.*, 69(1), 49–63, doi:10.1007/bf00375193, 1979.

808 Kuiper, K. F., Deino, A., Hilgen, F. J., Krijgsman, W., Renne, P. R. and Wijbrans, J. R.: Synchronizing Rock Clocks of
809 Earth History, *Science* (80-), 320(5875), 500–504, doi:10.1126/science.1154339, 2008.

810 Lee, J. K. W.: Ar–Ar and K–Ar Dating BT - *Encyclopedia of Scientific Dating Methods*, edited by W. Jack Rink and J. W.
811 Thompson, pp. 58–73, Springer Netherlands, Dordrecht., 2015.

812 Lee, J. Y., Marti, K., Severinghaus, J. P., Kawamura, K., Yoo, H. S., Lee, J. B. and Kim, J. S.: A redetermination of the

813 isotopic abundances of atmospheric Ar, *Geochim. Cosmochim. Acta*, 70(17), 4507–4512, doi:10.1016/j.gca.2006.06.1563,
814 2006.

815 Mark, D. F., Barfod, D., Stuart, F. M. and Imlach, J.: The ARGUS multicollector noble gas mass spectrometer: Performance
816 for $^{40}\text{Ar}/^{39}\text{Ar}$ geochronology, *Geochemistry, Geophys. Geosystems*, 10(10), 1–9, doi:10.1029/2009GC002643, 2009.

817 Matsuda, J., Senoh, K., Maruoka, T., Sato, H. and Mitropoulos, P.: K-Ar ages of the Aegean the volcanic rocks and arc-
818 trench system their implication for the arc-trench system, *Geochem. J.*, 33, 369–377, 1999.

819 McKenzie, D.: Active tectonics of the Alpine—Himalayan belt: the Aegean Sea and surrounding regions, *Geophys. J. Int.*,
820 55(1), 217–254, 1978.

821 Meulenkamp, J. E., Wortel, M. J. R., van Wamel, W. A., Spakman, W. and Hoogerduyn Strating, E.: On the Hellenic
822 subduction zone and the geodynamic evolution of Crete since the late Middle Miocene, *Tectonophysics*, 146(1–4), 203–215,
823 doi:10.1016/0040-1951(88)90091-1, 1988.

824 Min, K., Mundil, R., Renne, P. R. and Ludwig, K. R.: A test for systematic errors in $^{40}\text{Ar}/^{39}\text{Ar}$ geochronology, *Geochim.*
825 *Cosmochim. Acta*, 64(1), 73–98, 2000.

826 Nicholls, I. A.: Santorini volcano, greece - tectonic and petrochemical relationships with volcanics of the Aegean region,
827 *Tectonophysics*, 11(5), 377–385, doi:10.1016/0040-1951(71)90026-6, 1971.

828 Pe-Piper, G. and Piper, D. J. W.: The South Aegean active volcanic arc: relationships between magmatism and tectonics,
829 *Dev. Volcanol.*, 7(C), 113–133, doi:10.1016/S1871-644X(05)80034-8, 2005.

830 Pe-Piper, G. and Piper, D. J. W.: Neogene backarc volcanism of the Aegean: New insights into the relationship between
831 magmatism and tectonics, *Geol. Soc. Am. Spec. Pap.*, 418(02), 17–31, doi:10.1130/2007.2418(02), 2007.

832 Pe-Piper, G. and Piper, D. J. W.: The effect of changing regional tectonics on an arc volcano: Methana, Greece, *J. Volcanol.*
833 *Geotherm. Res.*, 260, 146–163, doi:10.1016/j.jvolgeores.2013.05.011, 2013.

834 Principe C, Arias A, Zoppi U.: Origin, transport and deposition of a debris avalanche de- posit of phreatic origin on Milos
835 Island (Greece). Montagne Pelee 1902-2002, Explosive Vol- canism in Subduction Zones, Martinique 12-16 May,
836 2002. Abstracts p. 71, 2002.

837 Raffi, I., Wade, B. S., Pälke, H., Beu, A. G., Cooper, R., Crundwell, M. P., Krijgsman, W., Moore, T., Raine, I. and
838 Sardella, R.: The Neogene Period, in *Geologic Time Scale 2020*, pp. 1141–1215, Elsevier., 2020.

839 Rinaldi, M. and Venuti, M. C.: The submarine eruption of the Bombarda volcano, Milos Island, Cyclades, Greece, *Bull.*
840 *Volcanol.*, 65(4), 282–293, doi:10.1007/s00445-002-0260-z, 2003.

841 Rivera, T. A., Storey, M., Zeeden, C., Hilgen, F. J. and Kuiper, K.: A refined astronomically calibrated $^{40}\text{Ar}/^{39}\text{Ar}$ age for
842 Fish Canyon sanidine, *Earth Planet. Sci. Lett.*, 311(3–4), 420–426, doi:10.1016/j.epsl.2011.09.017, 2011.

843 Rontogianni, S., Konstantinou, N. S., Melis, C. P. and Evangelidis: Slab stress field in the Hellenic subduction zone as
844 inferred from intermediate-depth earthquakes, *Earth, Planets Sp.*, 63(2), 139–144, doi:10.5047/eps.2010.11.011, 2011.

845 Schaen, A., Jicha, B., Hodges, K., Vermeesch, P., Stelten, M., Mercer, C., Phillips, D., Rivera, T., Jourdan, F., Matchan, E.,
846 Hemming, S., Morgan, L., Kelley, S., Cassata, W., Heizler, M., Vasconcelos, P., Benowitz, J., Koppers, A., Mark, D.,
847 Niespolo, E., Sprain, C., Hames, W., Kuiper, K., Turrin, B., Renne, P., Ross, J., Nomade, S., Guillou, H., Webb, L., Cohen,
848 B., Calvert, A., Joyce, N., Ganerød, M., Wijbrans, J., Ishizuka, O., He, H., Ramirez, A., Pfänder, J., Lopez-Martínez, M.,
849 Qiu, H. and Singer, B.: Interpreting and reporting $^{40}\text{Ar}/^{39}\text{Ar}$ geochronologic data, *GSA Bull.*, doi:10.1130/B35560.1, 2020.

850 Singer, B. S., Thompson, R. A., Dungan, M. A., Feeley, T. C., Nelson, S. T., Pickens, J. C., Brown, L. L., Wulff, A. W.,
851 Davidson, J. P. and Metzger, J.: Volcanism and erosion during the past 930 k.y. at the Tatara–San Pedro complex, Chilean
852 Andes, *Geol. Soc. Am. Bull.*, 109(2), 127–142, doi:10.1130/0016-7606(1997)109<0127:VAEDTP>2.3.CO;2, 1997.

853 Sonder, R. A.: Zur Geologie and Petrographie der Inselgruppe von Milos, *Zeitschr. Volc.*, 8, 11–231, 1924.

854 Spakman, W., Wortel, M. J. R. and Vlaar, N. J.: The Hellenic Subduction Zone: A tomographic image and its geodynamic
855 implications, *Geophys. Res. Lett.*, 15(1), 60–63, doi:10.1029/GL015i001p00060, 1988.

856 Stewart, A. L.: Volcanic Facies Architecture and Evolution of Milos, Greece, University of Tasmania., 2003.
857 Stewart, A. L. and McPhie, J.: Internal structure and emplacement of an Upper Pliocene dacite cryptodome, Milos Island,
858 Greece, *J. Volcanol. Geotherm. Res.*, 124(1–2), 129–148, doi:10.1016/S0377-0273(03)00074-X, 2003.
859 Stewart, A. L. and McPhie, J.: An Upper Pliocene coarse pumice breccia generated by a shallow submarine explosive
860 eruption, Milos, Greece, *Bull. Volcanol.*, 66(1), 15–28, doi:10.1007/s00445-003-0292-z, 2004.
861 Stewart, A. L. and McPhie, J.: Facies architecture and Late Pliocene – Pleistocene evolution of a felsic volcanic island,
862 Milos, Greece, *Bull. Volcanol.*, 68(7–8), 703–726, doi:10.1007/s00445-005-0045-2, 2006.
863 Traineau, H. and Dalabakis, P.: Mise en evidence d’une eruption phreatique historique sur l’île de Milos (Grece), *CR Acad*
864 *Sci Paris*, 1–38, 1989.
865 Vougioukalakis, G. E., Satow, C. G. and Druitt, T. H.: Volcanism of the South Aegean volcanic arc, *Elements*, 15(3), 159–
866 164, 2019.
867 Wendt, I. and Carl, C.: The statistical distribution of the mean squared weighted deviation, *Chem. Geol. Isot. Geosci. Sect.*,
868 86(4), 275–285, doi:10.1016/0168-9622(91)90010-T, 1991.
869 White, S. M., Crisp, J. A. and Spera, F. J.: Long-term volumetric eruption rates and magma budgets, *Geochemistry,*
870 *Geophys. Geosystems*, 7(3), 262–266, doi:10.1029/2005GC001002, 2006.
871 York, D.: Least squares fitting of a straight line with correlated errors, *Earth Planet. Sci. Lett.*, 5(C), 320–324,
872 doi:10.1016/s0012-821x(68)80059-7, 1968.
873